JOURNAL OF GEOPHYSICAL RESEARCH, VOL. 112, D09315, doi:10.1029/2006JD007476, 2007

Effects of resolution and model physics on tracer transports in the NASA Goddard Institute for Space Studies general circulation models

D. Rind,[1] J. Lerner,[1,2] J. Jonas,[1,2] and C. McLinden[1,3]

Received 3 May 2006; revised 26 October 2006; accepted 19 December 2006; published 15 May 2007.

[1] We explore the dependency of general circulation model tracer transports on model physics and horizontal and vertical resolution. We use NASA Goddard Institute for Space Studies (GISS) Model E at 4° × 5° with 20 and 23 layers and the GISS Global Climate Middle Atmosphere Model 3 at 4° × 5° with 23 and 53 layers and at 2° × 2.5° with 53 and 102 layers. The online tracers employed are CO_2, CH_4, N_2O, CFC-11, SF_6, ^{222}Rn, bomb ^{14}C, and O_3. Model experiments are done two ways: with specified stratospheric ozone or with the stratospheric ozone tracer used for atmospheric radiation calculations. The results show that when model physics produces greater precipitation over land in the Northern Hemisphere summer monsoon region, as occurs in Model 3, the associated dynamics (stronger Hadley cell) and subgrid-scale transports lead to faster and more realistic interhemispheric transport. Increased vertical resolution results in some increase in vertical mixing between the boundary layer and upper troposphere, due to both convective and synoptic-scale influences. A better resolved boundary layer does not result in higher surface concentrations, as the influence of various processes (convection, turbulence, rainfall) contribute in different ways. Transport into, within, and out of the stratosphere is faster (less realistic) with the coarser resolution models as wave forcing generates a stronger residual circulation. It is also faster in Model E as a result of its larger parameterized orographic gravity wave drag; the latter also results in a more ''leaky'' stratospheric tropical pipe. Horizontal resolution in this range by itself has minimal impact on most transports (although for active chemical tracers, photochemistry has been shown to be resolution-dependent). In contrast, finer vertical resolution leads to faster interhemispheric transport, slower mixing into and out of the stratosphere, and greater age of stratospheric air. When both resolutions are increased, the largest changes are seen. The interactive stratospheric ozone tracer, without an ozone hole parameterization, produced (as expected) greater ozone values than observations in the lower stratosphere. The associated temperature warming of a few degrees Celsius increased atmospheric stability and altered the tropospheric wave forcing of the Brewer Dobson circulation such that the stratospheric age of air increased by some 30%. This large sensitivity has implications for past and future stratospheric circulations and for the ability of climate perturbations to affect the stratosphere.

Citation: Rind, D., J. Lerner, J. Jonas, and C. McLinden (2007), Effects of resolution and model physics on tracer transports in the NASA Goddard Institute for Space Studies general circulation models, *J. Geophys. Res.*, *112*, D09315, doi:10.1029/2006JD007476.

1. Introduction

[2] There are an increasing number of model intercomparisons taking place, highlighted by the 20 coupled atmosphere-ocean models being evaluated in conjunction with the IPCC 2007 report. Included among the efforts are comparisons of tracer transports. For example, TransCom has as one of its goals ''to quantify and diagnose the uncertainty in inversion calculations of the global carbon budget that result from errors in simulated atmospheric transport.'' TransCom tracer transport comparisons have so far included CO_2 [*Law et al.*, 1996] for understanding the consequences of model differences for CO_2 inversions; and SF_6 [*Denning et al.*, 1999] for understanding interhemispheric transport. As the CO_2 example illustrates, tracer transports are important for understanding atmospheric composition changes that can affect climate; tropospheric ozone and dust are two other obvious species but with more complex chemistry and chemical sinks.

[3] Tracer transports resulting from atmospheric dynamics often involve ageostrophic or higher-order fields (e.g., eddy transports) that are hard to observe otherwise, so tracer

[1]NASA Goddard Institute for Space Studies, New York, New York, USA.
[2]Center for Climate Systems Research, Columbia University, New York, New York, USA.
[3]Meteorological Service of Canada, Downsview, Ontario, Canada.

0148-0227/07/2006JD007476$09.00

comparisons can theoretically improve this aspect of general circulation models (GCMs). Unfortunately, two factors have so far limited the utility of this approach. Observations of many of the relevant species are not yet available (for example, ^{222}Rn values in the upper troposphere, of interest for assessing convective fluxes). In addition, the models involved differ in many aspects, which complicates the assessment when results differ. It is this latter aspect which is the focus of the experiments reported here.

[4] Numerous papers have explored the impact of horizontal and/or vertical resolution on atmospheric simulations (an extensive but not all inclusive listing includes *Boer and Lazare* [1988], *Rind* [1988], *Boville* [1991], *Kiehl and Williamson* [1991], *Boyle* [1993], *Chen and Tribbia* [1993], *Gleckler and Taylor* [1993], *Sperber et al.* [1994], *Deque et al.* [1994], *Phillips et al.* [1995], *Williamson et al.* [1995], *Boer and Denis* [1997], *Williamson and Olsen* [1998], *Stendel and Roeckner* [1998], *Williamson* [1999], *Pope et al.* [2001], *Brankovic and Gregory* [2001], and *Roeckner et al.* [2006]). A general conclusion emerging from this work is that the biggest effect of increasing horizontal resolution on atmospheric dynamics emerges when going from >5° latitude × longitude (i.e., T21 in spectral models) to <3° (T42), with some additional improvement at ~2° (T63) [e.g., *Williamson et al.*, 1995; *Pope et al.*, 2001; *Roeckner et al.*, 2006]. At even finer resolution there is little systematic change especially in the extratropics, although tropical phenomena, including convection and Hadley cell intensity often continue varying, albeit somewhat inconsistently in different models [e.g., *Roeckner et al.*, 2006]. The results are also not independent of vertical resolution; for example, *Roeckner et al.* [2006] found that increasing vertical resolution from 2 km to 1 km improved dynamical simulations when the resolution was finer than 3°, while 2 km seemed sufficient at coarser horizontal scales. In the experiments reported here we investigate the impact on tracer transports of varying both the horizontal and vertical resolution around these ranges.

[5] Convective transports dominate the tropospheric vertical distribution of many short-lived species especially in the tropics [e.g., *Hess*, 2005]. Convection in particular is sensitive to resolution changes, with a tendency for increased convective fluxes and rainfall due to greater convergences when horizontal resolution is finer [e.g., *Brankovic and Gregory*, 2001]. In addition, increased vertical resolution can result in greater detrainment in the midtroposphere, with less deep convection above, altering the tropical temperature/stability profiles, including tropopause temperatures [*Pope et al.*, 2001; *Roeckner et al.*, 2006]. We have included in these experiments a model with very fine tropospheric vertical resolution to explore this possibility.

[6] As computer power has increased, climate models have been run with finer horizontal resolution. In the latest simulations for the IPCC Fourth Assessment Report, of the 23 contributing models, four models had resolutions in the 4°–5° range, eight around 3°, eight around 2°, and three less than 2°. Models incorporating atmospheric chemistry and its time-consuming photochemical routines tend to be of somewhat coarser resolution; of the 26 models participating in the 2000–2030 air quality assessments [*Dentener et al.*, 2006], twelve of the models use resolutions of 4°–5° or coarser, 14 use resolutions between 2.5° and 4°, and two use resolution around 2°. The model simulations performed here (at 2° × 2.5° and 4° × 5°) which focus on tracer transports of interest for atmospheric chemistry cover the majority of models in these ranges.

[7] The following section discusses the methodology for the experiments, while the results section discusses the models' interhemispheric and intrahemispheric transports, vertical mixing within the troposphere, transport between the troposphere and stratosphere, and within the stratosphere. Several of the model configurations use slightly different physics; in the discussion section we differentiate between the impact of altered physics and the influence of altered horizontal/vertical resolution on the tracer simulations. We also show how (inadvertently) correcting one of the major model deficiencies substantially improves many of the transport properties.

2. Methodology

[8] Through a series of systematic experiments, we investigate the dependency of tracer transports on model physics, horizontal resolution and vertical resolution with the use of six versions of NASA Goddard Institute for Space Studies (GISS) GCMs. The models are all new, in the sense that they have had substantial updates in their physics routines. They can be categorized into two main foci: "Model E," whose main use is for multicentury simulations of past and future climate, and "Model 3," which is the new version of the GISS Global Climate/Middle Atmosphere model, intended for investigating interactions between the stratosphere and troposphere. Each of the different configurations has its own intended purposes, which along with other information is provided in Table 1.

2.1. Updates Common to Both Model E and Model 3

[9] The updated physics routines common to both models are discussed in detail by [*Schmidt et al.*, 2006]. Of particular relevance for tracer transports, atmospheric turbulence is calculated throughout the whole atmosphere (instead of using dry convection to remove unstable gradients). In the boundary layer a formulation is used for the temperature, moisture and scalar fluxes that consists of a local (diffusive) term and a countergradient term derived from large-eddy simulation (LES) data [*Holtslag and Moeng*, 1991]; in addition, there is a revised formulation for turbulent kinetic energy derived by *Moeng and Sullivan* [1994] from LES data. The approach includes a nonlocal turbulence model whose primary effect is to lift tracers (including water vapor) from the lowest to higher levels of the boundary layer. Above the boundary layer a new second-order closure model is employed [*Cheng et al.*, 2002; *Canuto and Dubovikov*, 1996a, 1996b] which alters the solution of the Reynolds stress and heat flux equations, and increases the critical Richardson number for cessation of turbulence from 0.2 to 1; this has the effect of improving species distributions in unstable conditions [*Schmidt et al.*, 2006]. In conjunction, additional alterations were made to the surface flux calculations (see *Schmidt et al.* [2006] for details). These changes will influence the vertical distribution of species, especially those with surface/boundary layer sources.

Table 1. Characteristics of the GISS Models Used for These Comparisons[a]

Name	Model	Vertical Resolution, km				Comment
		PBL	Troposphere	Stratosphere	Mesosphere	
E20 (E20i)	Model E 4° × 5°	0.4	1.0–2.0	2.0–8.0	NA	For long-term climate studies; lower model top; Rayleigh friction for stratospheric drag
E23 (E23i)	Model E 4° × 5°	0.4	1.0–1.5	2.0–8.0	10	Long-term studies with stratospheric forcing; strong orographic gravity wave drag in lower stratosphere
M23 (M23i)	Model 3 4° × 5°	0.4	1.0–1.5	2.0–8.0	10	Tropospheric chemistry studies with stratospheric interaction; differs from E23 because of weaker gravity wave drag, altered convective, and cloud and boundary layer parameterizations
M53 (M53i)	Model 3 4° × 5°	0.3	0.5	1.0–3.0	4	With better resolution in upper stratosphere/mesosphere more appropriate for decadal solar UV/ozone studies
F53 (F53i)	Model 3 2° × 2.5°	0.3	0.5	1.0–3.0	4	New standard model for stratosphere-troposphere climate interactions
F102	Model 3 2° × 2.5°	0.2	0.3	0.4–1.4	2–3	For high vertical resolution studies (solar forcing, QBO)

[a]Resolution for the different levels is given in km. The letter designation "i" indicates that the model atmospheric radiation utilizes (interacts with) the tracer ozone rather than prescribed values. NA means not applicable.

[10] The convection routine has also been modified. It still uses a mass flux approach to cumulus parameterization with one undiluted and one entraining plume, with the closure assumption that sufficient mass is transported to produce neutral buoyancy of lifted parcels in one time step. Downdrafts are now handled in a more sophisticated manner, including entrainment. Cumulus condensate is detrained into an anvil which evolves in a similar manner to stratiform clouds. All moisture advection in this model is done with a quadratic upstream scheme (QUS) (similar to the second-order moments scheme of *Prather* [1986]), and that now includes compensatory subsidence in response to convection. These changes will have their biggest direct impact on convective mixing of tracers, including the levels of detrainment.

[11] Other updates from previous versions that are common to both models occur in their radiation scheme (more correlated k intervals), land surface (new snow hydrology and vegetation characteristics), stratiform cloud calculation, and numerics (for increased numerical stability at the pole). These affect passive tracers by influencing the temperature gradients and winds in the climate simulation.

[12] Of direct relevance for tracer transport, all tracers are still advected with the nondiffusive QUS scheme which involves saving nine subgrid-scale moments as well as the mean within each grid box. This approach increases the effective resolution of the tracer fields; the effective tracer resolution for the model with 4° × 5° horizontal gridding is ~1.3° × 1.6°, while for 2° × 2.5° grids, it is ~0.7° × 0.8° [*Schmidt et al.*, 2006, Table 1]. In the new models, the tracers are much more consistent with the basic model physics; for example, the moist convection routine has been adapted to be locally and globally tracer mass conserving, and the various components of the convective fluxes alter the second-order moments in a consistent fashion.

2.2. Updates That Differ Between Model E and Model 3

[13] Within this general similarity, Model E and Model 3 have some differences in model physics which will be shown to be important as far as tracer transport is concerned. Different choices have been made in the boundary layer (Model 3 uses virtual potential temperature), and cloud and convection schemes (e.g., downdraft entrainment, cloud liquid water evaporation). The differences result in the cloud liquid water content being some 70% larger in E23 than in M23 (as indicated in Table 1, letter E refers to Model E; M refers to the 4° × 5° version of Model 3; and the number indicates the vertical layers). GISS models have previously been shown to overestimate cloud optical thicknesses [*Tselioudis and Jakob*, 2002] so the Model 3 values would seem to be an improvement. To achieve model radiation balance, the total cloud cover is slightly higher in M23 (61% compared with 59% due to a lower threshold relative humidity), and so its albedo is also slightly higher (30.9% compared with 29.4%). While the global net radiation at the top of the atmosphere and at the surface is essentially the same (close to zero) in both models, it is larger over the ocean in M23 (by ~5 W m^{-2}), and larger over land in E23 (by ~8 W m^{-2}). Both are improvements in M23 (see *Schmidt et al.* [2006] for comparisons of Model E with observations for these fields), and, as we will see, this impacts the precipitation field and various transports.

[14] Given that Model E is specifically designed for multicentury simulations, it has been primarily used to this point in time at 4° × 5° resolution (for example, in the IPCC runs for AR4). It comes in two versions with either 20 or 23 levels (henceforth E20, E23), which differ not only in their vertical layering but by the location of the model top: at 0.1mb for E20, and 0.002 mbar for E23. They also differ in their gravity wave drag formulations, as discussed below. Both versions are being used extensively at GISS, with numerous publications. Model 3 in contrast is designed for evaluating troposphere/stratosphere interactions, and in general utilizes finer resolution. The lowest-resolution version (M23) matches that of model E, while other versions contain finer vertical layering (M53), finer horizontal resolution (2° × 2.5°) (F53) and both finer horizontal and vertical spacing (F102). See Table 1 for the distribution of the vertical layering. All Model 3 versions have their top at 0.002 mbar. It too is being used for a variety of experiments, often involving atmospheric chemistry [e.g., *Wu et al.*, 2007].

[15] The models also differ in their gravity wave drag. Model 3 utilizes the formulations discussed by *Rind et al.* [1988, 1999] except with much smaller values. These

Table 2. Three-Dimensional Interhemispheric Transport Time (τ) in the Different Models[a]

Model	SF_6, years	CFC-11, years	CH_4, years
F102	0.78 ± 0.03 [0.83 ± 0.03]	0.55 ± 0.06 [0.71 ± 0.04]	0.61 ± 0.03 [0.65 ± 0.02]
F53	1.02 ± 0.03 [1.10 ± 0.04]	0.72 ± 0.03 [0.89 ± 0.06]	0.82 ± 0.03 [0.84 ± 0.03]
M53	1.01 ± 0.03 [1.04 ± 0.02]	0.79 ± 0.04 [0.90 ± 0.05]	0.85 ± 0.04 [0.85 ± 0.02]
M23	1.11 ± 0.03 [1.16 ± 0.03]	0.93 ± 0.04 [1.03 ± 0.05]	0.95 ± 0.02 [0.98 ± 0.04]
E23	1.33 ± 0.04 [1.34 ± 0.03]	1.21 ± 0.06 [1.31 ± 0.05]	1.15 ± 0.05 [1.14 ± 0.03]
E20	1.21 ± 0.05 [1.25 ± 0.03]	0.96 ± 0.04 [1.13 ± 0.06]	1.03 ± 0.04 [1.00 ± 0.04]

[a]The interannual standard deviation is also shown. Results from the "interactive" runs are shown in brackets.

include explicit sources for both the orographic and nonorographic (from shear, convection and frontogenesis) parameterized gravity waves, with vertical propagation based on linear saturation theory through the ambient background wind and temperature structure. E23 has similar formulations, except it still uses the previous, larger values. E20 uses a Rayleigh friction formulation, with coefficients to mimic the net drag in E23. As model E was not primarily designed for stratospheric studies, less effort has been expanded on its stratospheric simulations, a point that will become apparent in the tracer transport comparisons. Gravity wave drag remains an uncertain parameterization for middle atmosphere models and is often calibrated to produce the proper wind and temperature fields in the stratosphere (which is why model E uses strong gravity wave drag). This does not guarantee it will have the proper effect on tracers, however.

[16] E23 and M23 differ only in their model physics, M53 and F53 differ only in their horizontal resolution, while M23 and M53, and F53 and F102 differ in their vertical resolution. Such comparisons should thus allow us to assess the impact of these changes on various tracer transports, at least within the context of these models.

2.3. Online Tracers and Experiments

[17] The online tracers that we use for these calculations have all been discussed in previous publications: CO_2, CH_4, N_2O, CFC-11, SF_6, ^{222}Rn, bomb ^{14}C, and O_3. See *Rind and Lerner* [1996] and *Rind et al.* [1999, 2001, 2002] for their sources and sinks (especially Table 1a of *Rind et al.* [2001]). The linearized ozone photochemistry (Linoz) of *McLinden et al.* [2000] is employed in the stratosphere. A similar approach is taken for the other tracers with stratospheric photochemistry (CH_4, N_2O, CFC-11) [*McLinden et al.*, 2000; *Olsen et al.*, 2001; *Hannegan et al.*, 1998]. In the troposphere, CH_4 photochemistry is parameterized as in work by *Fung et al.* [1991]. Tropospheric ozone is calculated using monthly mean ozone production and loss rates archived from GEOS-CHEM, a global photochemical transport model [*Bey et al.*, 2001; *Park et al.*, 2004].

[18] CO_2, CH_4, N_2O, and CFC-11, all of which have been run previously, all started from observed initial conditions circa 1980s to mid-1990s on the basis of tropospheric observations and UARS data in the stratosphere (D. Shindell, 1999, personal communication). SF_6 and ^{222}Rn started from near zero conditions everywhere. ^{14}C was input following the prescription of *Johnston* [1989]. Stratospheric ozone started from the observed SAGE II climatology [*Rind et al.*, 2005], while tropospheric ozone was set to 20 ppbv. Following a three month spin-up, each of these models with online tracers has been run for 12 model years. Results for each year are compared to determine when the particular tracer has reached equilibrium; for most of the tracers it is after the first or second year in the troposphere, and the third year in the stratosphere. Exceptions are CO_2, CFC-11 and SF_6 which are continually increasing because of their sources. For all of the tracers, the relevant calculations are performed each year (e.g., interhemispheric transport) and only the "stabilized" transport values are utilized. The remaining $\sim$9–10 years is sufficiently long to establish their transport characteristics (as shown by *Hall et al.* [1999], this is true even for the age of air in the stratosphere).

[19] In the course of the experiments, a particularly strong influence on model transports was uncovered involving stratospheric ozone. This led to our running all the simulations twice. In the first set, the atmospheric radiation is calculated using the input (observed) stratospheric ozone field. In the second set, the experiments are rerun using the stratospheric ozone that results from the ozone tracer field, hence the radiation is interactive with the stratospheric ozone tracer (such runs are given by the letter designation "i" in Table 1 and elsewhere in the text).

[20] The significance of differences between experiments reported here is determined by comparison with the interannual standard deviations for the respective models and by comparison between the interactive and noninteractive ozone simulations. In cases where the ozone radiation interaction clearly does not have an influence, the two sets of runs help provide consistency checks on the relative results from the different models.

3. Results

3.1. Interhemispheric Transport

[21] For interhemispheric transport (IHT), we use tracers whose primary source is in the Northern Hemisphere: CFC-11, CH_4 and SF_6. The IHT is calculated by taking the difference in concentration between the two hemispheres divided by the transport across the equator, i.e., the timescale for hemispheric equilibration. The resulting transport time τ is correct only if the Southern Hemisphere source is negligible; as the Southern Hemisphere sources in these runs contribute 8% to the SF_6 and CFC-11, and 1% for methane (considering both the sources and chemistry sinks), we increase the transport times accordingly.

[22] The results for the different models are shown in Table 2. There is a range of close to a factor of two for CFC-11 and CH_4 between the finest resolution model (F102) which has the shortest transport times, and E23, which has the longest. The horizontal resolution is not the dominant factor in this difference, as M53 and F53 have very similar values. Model E in general has somewhat longer transport times.

Table 3. Partitioning of Interhemispheric Transport in the Different Models (From SF_6 Transports), Tropical Eddy Kinetic Energy, and Mean Circulation[a]

	Units	F102	F53	M53	M23	E23	E20
MMC contribution to IHT	%	45 [45]	41 [40]	38 [37]	42 [40]	44 [43]	45 [44]
EDDY contribution to IHT	%	55 [55]	59 [60]	62 [63]	58 [60]	56 [57]	55 [56]
Tropical standing EKE	10^{16} J	184 [182]	136 [134]	161 [153]	142 [142]	122 [123]	120 [121]
Tropical transient EKE	10^{16} J	408 [402]	258 [258]	321 [338]	289 [279]	244 [228]	248 [249]
Hadley cell peak (D–F)	10^9 kg s^{-1}	−203 [−204]	−179 [−177]	−211 [−208]	−179 [−174]	−165 [−163]	−166 [−161]
Hadley cell peak (J–A)	10^9 kg s^{-1}	295 [288]	238 [227]	240 [228]	217 [227]	203 [202]	205 [204]
Precipitation at 18°N, J–A, land	mm d^{-1}	8.0 [8.3]	9.0 [9.3]	6.4 [6.1]	5.8 [6.4]	5.7 [5.6]	5.0 [5.0]

[a]Results from the "interactive" runs are shown in brackets.

The same relative changes are found for the interactive runs (in brackets), which have a tendency for slightly longer IHTs, especially for CFC-11.

[23] How does IHT occur in the real world? Upper level convective divergent outflow has been suggested as the principal mechanism of IHT [*Prather et al.*, 1987; *Hartley and Black*, 1995], including convection over land regions (e.g., Amazon, equatorial Africa, India) [*Lintner*, 2003]. As noted by *Denning et al.* [1999], vertical transport is critical for IHT, as the equatorward motion that transports air from the northern to southern hemispheres occurs in the upper troposphere during June–August. The reversed vertical gradient of tracer in the low latitudes of the Southern Hemisphere suggests that the bulk of interhemispheric transport occurs aloft [e.g., *Plumb and Mahlman*, 1987; *Plumb and McConalogue*, 1988]. *Staudt et al.* [2001] estimated from modeling studies that up to ~ 75% of total interhemispheric transport occurred in the upper troposphere. Model studies [e.g., *Denning et al.*, 1999] have found transport across the equator roughly equally divided among the mean meridional circulation (MMC), stationary eddies and transient eddies, therefore ~2/3 by eddies.

[24] Modern dynamic meteorology recognizes that the separation between the mean circulation and eddies is to some extent misleading [e.g., *Andrews and McIntyre*, 1976]. This is particularly true in the stratosphere, where the mean circulation is largely driven by eddy flux convergences; furthermore, in that regime, conservative, frictional and diabatic processes are more likely to be small, producing cancellations in eddy and mean circulation transports [*Andrews et al.*, 1987] with potentially large misleading terms for each. Therefore stratospheric transports (sections 3.6, 3.7 and to some extent 3.4 and 3.5) will be discussed in terms of the transformed Eulerian mean (TEM) residual circulation, which is a more accurate depiction of the mean circulation plus eddy effects, especially for linear, steady, conservative waves [e.g., *Andrews et al.*, 1987]. In the troposphere, the mean circulation is driven by diabatic forcing, e.g., convective latent heat release, with the eddy contribution quite limited [see, e.g., *Crawford and Sasamori*, 1981]. Similarly, the primary forcing for eddies (baroclinic instability) is largely independent of zonal mean meridional circulation effects. Therefore, for tropical and tropospheric phenomena, we will continue to differentiate between eddies and the mean circulation components of transport. This has the advantage of allowing for direct comparison with previous studies, which used these concepts. In addition, the two phenomena may have very different sensitivity to changes in physics or resolution. For both the Eulerian and TEM descriptions, however, transport ultimately depends on departures from steady, linear, conservative (nondiabatic, frictionless) conditions [*Andrews et al.*, 1987].

[25] We can compare the model results with the real world expectations, which will also help explain why the Model E transport times are slower. In terms of the proportion of southward transport of SF_6 mass flux across the equator, the Model 3 and Model E configurations all have between 75% and 90% at levels above 500 mbar. The proportion of total vertical transport above 500mb associated with moist convection (as opposed to large-scale transport) ranges between 60–70% in M53, F53, and F102; it is 54% in M23, and about 45% in E20 and E23. Model E has reduced convection and precipitation over land in the Northern Hemisphere summer monsoon region (see Table 3). This affects the mean circulation: model E has the weakest Hadley cell (and F102 the strongest, Table 3). It also affects the tropical eddy kinetic energy (EKE) by altering the dynamic generation; the tropical EKE is being

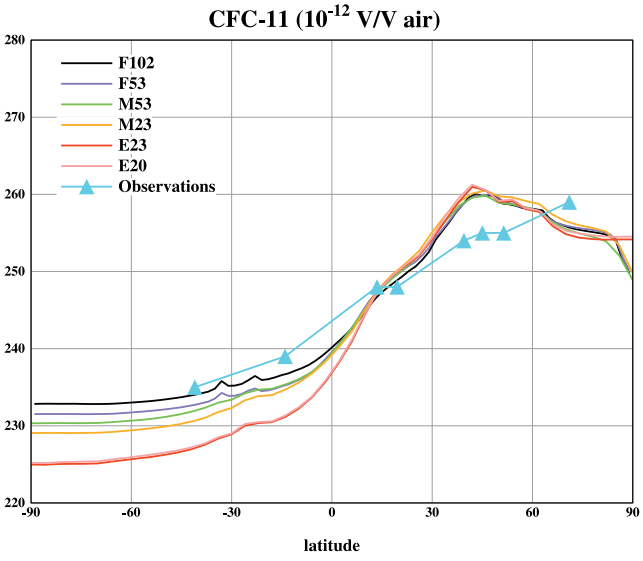

Figure 1. Comparison of model CFC-11 distributions with observations [*Kaye et al.*, 1994] during the time when the strong increase in the source strength corresponded to that used in the model experiments. Observations are at specific locations, and model values are zonal averages. The conclusions are similar when using model results for the specific locations.

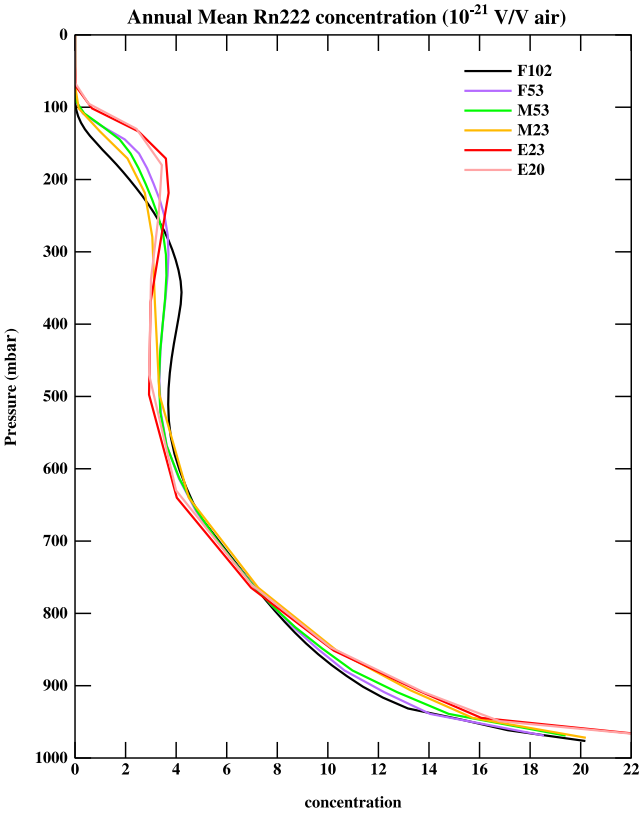

Figure 2. Global annual average distribution of ^{222}Rn in the different models.

generated in all of the models via conversion of eddy available potential energy (EAPE), and both EAPE and this conversion are weakest in model E (while, again, F102 has the largest). Potential energy at low latitudes is generated when the latent heat release occurs in warmer air; because of the choices noted in section 2.2, Model E has a lower proportion of precipitation over (warm) land compared with that over the (cooler) ocean than does Model 3. The biggest difference in EKE between Model E and Model 3 is in the tropical upper troposphere, directly influencing IHT. As both the Hadley cell and eddy kinetic energy change in the same way between models, eddy/mean circulation transport ratios range between 55% and 65%, close to the general model value in the TransCom comparisons.

[26] In contrast to these results, *Williamson et al.* [1995] found that tropical upper tropospheric EKE decreased with increasing resolution (without increasing vertical resolution) in the CCM2 model with no evidence of convergence up to 1° resolution; *Brankovic and Gregory* [2001] found little systematic change when increasing the resolution from 2° to 0.6° (again without increasing the vertical layering). The combination of finer horizontal and extremely fine vertical resolution may aid the GISS model in its generation of tropical EKE. In addition, in all of the GISS models, convection mixes momentum (which then acts as a sink for EKE), and we show later that at the highest altitudes in the tropical upper troposphere, Model E has the largest convective flux, and F102 the least.

[27] What is the proper IHT? Observations of passive tracers indicate a timescale ranging from 0.7 to 1.8 years [*Lintner*, 2003], with values often recorded around 1 year [e.g., *Gilliland*, 1997; *Kjellstrom et al.*, 2000]. However, interhemispheric transport times calculated from surface observations (as is often the case) will generally exceed those using the full depth of the atmosphere (three-dimensional (3-D), as in these calculations) [*Levin and Hesshaimer*, 1996] because of the relaxed gradients in passive tracers found at altitudes above the surface; the difference is about a factor of two [*Lintner*, 2003]. Indeed, in the models used here, the surface interhemispheric difference is about twice that for the troposphere as a whole. The exchange time for the NCEP reanalysis winds utilized in the MATCH model is about 0.8 years (for CFC-11), when employing the full 3-D data [*Lintner*, 2003]. The 3-D exchange time in the models used for the TRANSCOM SF_6 intercomparison [*Denning et al.*, 1999] generally ranged from 0.55 to 1.05, with an average of 0.81 ± 0.2. From this perspective, the Model E values look to be too slow.

[28] Considering the tropospheric circulation, during June–August, estimated values of the Hadley cell range from a peak of ~190 × 10^9 kg s^{-1} in the NCEP/NCAR reanalysis to ~230 × 10^9 kg s^{-1} in the older ECMWF analysis [*Trenberth et al.*, 2000], to 270 × 10^9 kg s^{-1} in the latest ERA40 reanalysis [*Kållberg et al.*, 2005]. The various models generally produce values within this range, although F102 is higher than even the ERA40 estimate. For precipitation, the various observational data sets [*Shea*, 1986; *Legates and Willmott*, 1990; *Hulme*, 1992; *Beck et al.*, 2005], peak at a little over 10 mm d^{-1} in July in Northern India, and 6–10 mm d^{-1} over Central America. Model 3 values generally are similar to observed over Central America. They are also similar or close to the upper end of the observed values over northern India, especially in the finer resolution runs in which the largest values occur, perhaps aided by the increased topography. Model E precipitation is generally lower over Central America (3–6 mm d^{-1}) and in E20, lower over northern India (6–10 mm d^{-1}).

[29] We can compare the model results with observations of CFC-11 made during the time of the strong trend used as the source in these experiments [*Kaye et al.*, 1994]. The results are shown in Figure 1; the reduced gradient characteristic of the models with the shorter IHT times is a better fit with the observations (which actually imply an even faster IHT). The model results are for latitudinal averages while the observations are at specific locations, but the conclusions are similar when using the model values for the

Table 4. Model Global Results Related to ^{222}Rn Vertical Distribution[a]

Model	Ratio 350–200 mbar/ 984–844 mbar	Vertically Integrated Convective Mass Flux, 10^9 kg s^{-1}	Global Eddy Kinetic Energy, 10^{17} J
F102	0.280 [0.280]	1429 [1421]	3728 [3683]
F53	0.286 [0.288]	1568 [1563]	3282 [3225]
M53	0.261 [0.260]	1720 [1712]	3259 [3257]
M23	0.226 [0.226]	1323 [1318]	3049 [3021]
E23	0.244 [0.241]	1228 [1232]	3234 [3261]
E20	0.230 [0.227]	1165 [1170]	3241 [3239]

[a]Results from the "interactive" runs are shown in brackets.

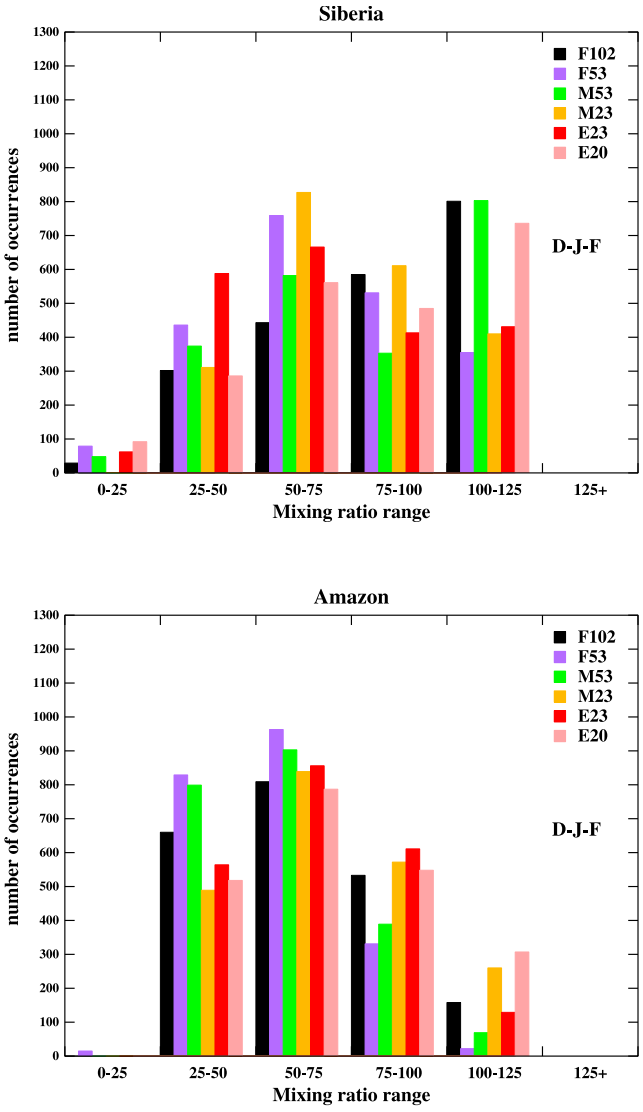

Figure 3. Histogram of hourly radon concentration values during December–February in a representative model year for grid boxes in (top) Siberia and in (bottom) the Amazon rainforest.

relevant grid boxes. A caveat is that results from any particular period may not be indicative of general conditions.

3.2. Intrahemispheric Transport

[30] The mixing within each hemisphere is primarily a function of eddy transports from the midlatitude sources, with subsequent involvement of the mean circulation. The standard deviation between the models of the eddy kinetic energy in the Northern Hemisphere troposphere is ~6%. All the models produce a ratio between the midlatitude and equatorial region concentrations for CFC-11 of 1.10–1.14. Observed values for this ratio covering the analogous time period for the 1980s are ~1.10 [*Kaye et al.*, 1994]. Observed values for the SF_6 ratio in the marine boundary layer are similar (~1.06) [*Denning et al.*, 1999], while ratios for Kr85 are again of roughly similar magnitude (~1.16) [*Jacob et al.*, 1987].

[31] Concerning the midlatitude/high latitude ratio, all the models in this study produce similar values at the surface of ~1.08 ± 0.01, which is slightly higher than indicated by the sparse observations shown by *Denning et al.* [1999] (~1.02) for an Atlantic transact during two months. Whether this represents inadequate mixing or insufficient observational evidence is unknown, although Model E underestimates storm track frequencies at the highest latitudes [*Schmidt et al.*, 2006, Figure 19] which might be indicative of a lack of sufficient transport. In the Northern Hemisphere, the similarity in extratropical EKE leads to similar intrahemispheric mixing properties in all the models.

[32] In the Southern Hemisphere, most of the models have similar magnitudes of EKE except for F102, which has about 15–20% more. There is some variation among the models in the difference in gradient between midlatitudes and the pole, but it is not consistent from tracer to tracer. For example, there is a difference in CFC-11 gradient (with F102 having the least), but not in SF_6 or CO_2. Observations show little extratropical gradient in the Southern Hemisphere for SF_6, CO_2 or CFC-11 [*Denning et al.*, 1999] (NOAA CMDL sampling network (http://cdiac.ornl.gov/trends/co2/cmdl-flask/cmdl-flask.html), and overall the model gradients are small as well.

3.3. Vertical Mixing Within the Troposphere

3.3.1. Mixing Between the Boundary Layer and Free Troposphere

[33] We use ^{222}Rn to assess vertical mixing for short-lived species within the troposphere. Because of its short lifetime (5 day *e*-folding time for radioactive decay) its distribution emphasizes the convective fluxes and other rapid transport processes in models. Observations are not yet capable of providing firm constraints on its vertical mixing, especially in the tropics, but the tracer is useful in comparing different models, convection schemes and resolutions [e.g., *Intergovernmental Panel on Climate Change* (*IPCC*), 1995]. Previous studies have underscored the sensitivity of this tracer to the convective parameterization, and experiments have shown that changes in horizontal/vertical resolution affect model convection.

[34] Shown in Figure 2 is the global, annual average vertical profile of ^{222}Rn from the different models. The results indicate that the distributions on this scale are quite similar. Concerning the differences which do arise, the two Model E runs have somewhat lower values between 500 and 300 mbar, where F102 has the largest, and Model E has somewhat higher values at levels above 200 mbar, where F102 has the smallest. In all the models, both large-scale vertical transport and moist convection remove ^{222}Rn from

Table 5. Percent of Species Above the 100 mbar Level[a]

Model	CFC-11	CH_4	N_2O	SF_6
F102	5.27 [5.01]	8.59 [8.37]	8.13 [7.85]	7.19 [6.74]
F53	5.37 [5.03]	8.84 [8.56]	8.35 [8.03]	7.60 [7.06]
M53	5.45 [5.10]	8.86 [8.56]	8.37 [8.02]	7.78 [7.22]
M23	5.52 [5.16]	8.92 [8.62]	8.44 [8.09]	8.16 [7.63]
E23	5.81 [5.52]	9.08 [8.87]	8.64 [8.40]	8.29 [7.90]
E20	5.86 [5.61]	8.96 [8.75]	8.50 [8.24]	8.42 [8.10]

[a]Results from the "interactive" runs are shown in brackets.

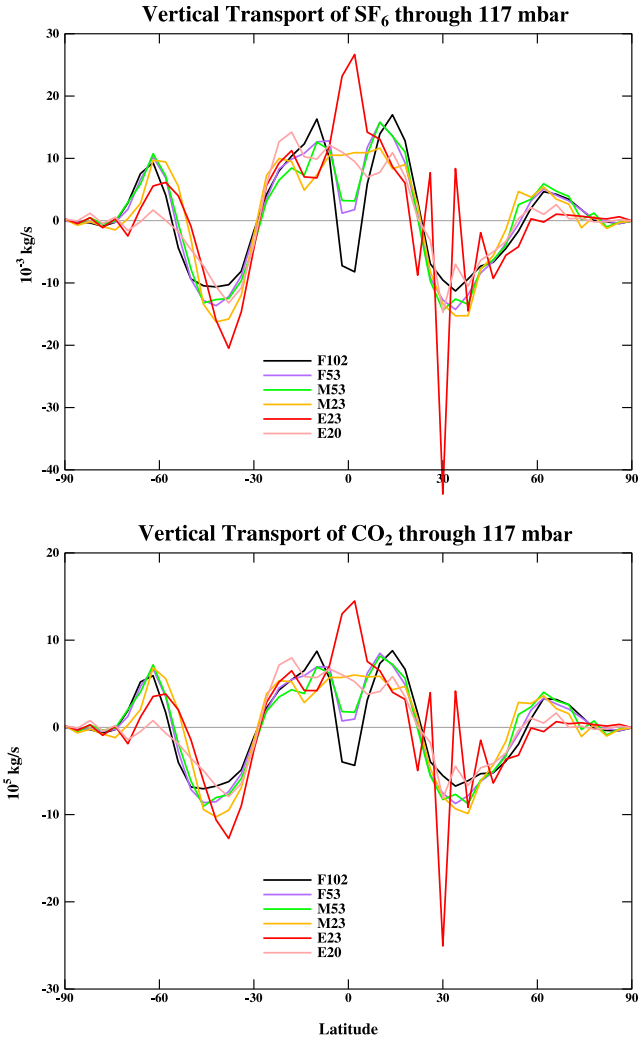

Figure 4. Annual vertical transport through 117 mbar by the large-scale dynamics for (top) SF_6 and (bottom) CO_2.

the region below 800 mbar. The large-scale transport then dominates in lifting ^{222}Rn up to about 500 mbar, and then convective transport dominates above, although both are generally positive throughout. Ultimately, the relatively small differences seen in this vertical profile are due to differences in convective mixing, associated with both model physics and vertical resolution.

[35] We show in Table 4 the ratio of ^{222}Rn between the upper troposphere (350–200 mbar) and the lower troposphere (984–444 mbar, primarily in the boundary layer) The lower-resolution models, including both model E runs, all have reduced values, indicating less vertical mixing. The vertically integrated convective mass flux in Table 4 indicates that the runs with reduced vertical mixing have reduced mass flux as well. Increased vertical eddy transports arise in the finest resolution model, due to both its higher EKE (Table 4) as well as the likely better resolution of the warm conveyor belt in synoptic systems [e.g., *Hess*, 2005].

[36] These results differ from those reported by *Pope et al.* [2001] and *Roeckner et al.* [2006] who found that finer vertical resolution led to reduced vertical mixing into the upper troposphere (for water vapor). In those simulations, the finer vertical resolution was associated with increased midlevel convective detrainment, which stabilized the atmosphere and prevented deeper convection from occurring as frequently. In this model the reduced convective penetration with finer vertical resolution occurs only at levels above 200 mbar (as indicated several paragraphs above). The differences may relate to the particularities of the convection scheme. In addition, *Pope et al.* [2001] note that models with semi-Lagrangian advection schemes show less sensitivity to vertical resolution for moisture; as this model uses the highly nondiffusive second-order moments scheme for vertical advection it should have less implicit numerical diffusion associated with coarser vertical resolution.

[37] The results can be compared in a general way with other modeling studies of ^{222}Rn. For example, *Mahowald et al.* [1997] used the MATCH model with winds provided by NCEP and ECMWF. In the Northern Hemisphere, the ratio of concentration at 300mb to that at low levels at upper midlatitudes varied from 20% (NCEP winds) to 12% (ECMWF data). The finer resolution models used here (M53, F53, F102) all had ratios around 13%, close to the ECMWF value, while the values with the coarser resolution models were lower (M23, 9.7%; E23, 9.2% and E20, 7.1%). However, the MATCH model overpredicted the upper troposphere values in comparison with specific observations, by about 2.5; if one were to apply that to the simulations in general, it would reduce the "observed" ratio to 5–8% (assuming the source was not similarly overpredicted). Note that the experiments in this paper use a source for ^{222}Rn associated with decay of radium in soils as well as a small contribution from the oceans [*Rind and Lerner*, 1996; *Taguchi et al.*, 2002]; the soil contribution is a function of temperature (and set to zero when the ground is frozen or snow covered), but not water saturation.

[38] *Mahowald et al.* [1997] found that results are very sensitive to model convection schemes. The GCMs discussed here all use a similar scheme, albeit with somewhat different choices, hence their results do not differ as much

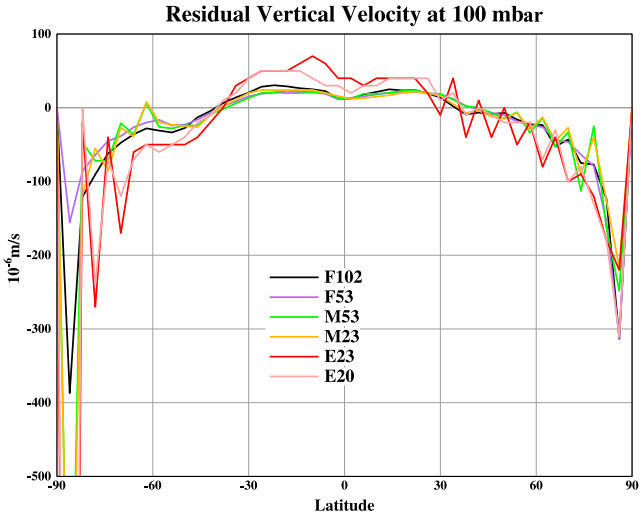

Figure 5. Annual average $\overline{w}^*$ as a function of latitude at the 100 mbar level.

Table 6. Residence Time for Bomb ^{14}C in the Stratosphere and Net Ozone Transport[a]

Model	Bomb ^{14}C Residence Time First 36 Months, years	Bomb ^{14}C Residence Time 90 Months, years	Net Ozone Transport Through 117 mbar, Tg yr^{-1}
F102	3.75 [4.08]	4.42 [4.92]	536 [454]
F53	3.03 [3.64]	4.00 [4.50]	643 [514]
M53	2.98 [3.68]	3.86 [4.47]	678 [533]
M23	2.73 [3.30]	3.67 [4.11]	801 [634]
E23	2.73 [3.23]	4.15 [4.52]	902 [725]
E20	2.78 [3.24]	3.81 [4.07]	855 [706]

[a]Results from the "interactive" runs are shown in brackets.

from one another as have occurred in other model comparisons (e.g., the 20 models of *IPCC* [1995]).

3.3.2. Boundary Layer Concentrations and Processes

[39] Another use of ^{222}Rn, or in fact any of the tracers, would be to investigate the impact of finer vertical resolution on boundary layer mixing, both diurnal and seasonal. With thinner layers in the boundary layer, models might be expected to have increased tracer concentrations from a surface source especially at night, when the atmosphere is stable, and perhaps in winter. However, with its land surface source a function of temperature, ^{222}Rn will have reduced emissions during winter, especially when the soil is frozen. The seasonal variation of rainfall in the models will influence the source as well, by affecting the ground surface temperature. Vertical resolution will also affect turbulent transports and convective mixing, making it unclear what role it will really play.

[40] The model results show no systematic seasonal variation in boundary layer concentrations with either model physics or resolution; apparently the various processes work against one another. In comparison with observations made at Chester, Pennsylvania [*Jacob and Prather*, 1990], only F102 produced the appropriate summer peak, with the proper magnitude. However, at other locations in the United States the seasonal peak is not necessarily in summer [*Jacob and Prather*, 1990], so the comparison for any particular region may not be generally applicable. The salient point is that the magnitude of the surface concentration is not a function of vertical resolution in these models.

[41] We can also compare the diurnal variation. Concerning the ratio between maximum and minimum concentration, all the runs have ratios close to the observed, especially during winter. The time of concentration peak and trough are a few hours later than the observed; however, in both the model and observations the peaks and troughs are quite broad, and the differences may not be meaningful. This conclusion was true for a wide diversity of locations.

[42] As an additional assessment of the influence of vertical resolution on low-level concentrations, the hourly values were composited into histograms of occurrences for various regions. Shown in Figure 3 are the results for two diverse situations: Siberia in winter where a reduced source would occur in conjunction with a stable atmosphere; and the Amazon rainforest region during the rainy season, where a strong source would be combined with convective activity and rainfall. In neither case is there any consistent relationship between vertical resolution and peak or minimum in concentration. Apparently, the numerous other influences, including convection and turbulent transports, and the rainfall and cloud cover influence on ground temperature, prevent the finer resolution from resulting in higher concentrations in any consistent manner. For example, E20 has high values presumably because it has reduced convection over land.

[43] We also investigated the variation in the planetary boundary layer depth (PBLD) at different locations. PBLD is determined by calculating the altitude at which the turbulent kinetic energy decreases to 10% of its surface value. There is no correlation between either the maximum or minimum PBLD and vertical or horizontal resolution. Model E values, due to choices associated with the planetary boundary layer and convective parameterizations, have nighttime minimum values as shallow as the finest resolution versions of Model 3 on the time average. All the models may underestimate the daily maximum, and the use of 5% turbulent kinetic energy as the criterion increases the PBDL appropriately (L. Mickley, personal communication, 2006). However, this choice has a negative impact on the diurnal variation, raising the nighttime values unrealistically.

[44] The surface wind values are of importance for both evaporation and surface fluxes including dust. There is some increase in velocity with finer resolution (more so horizontal than vertical). Even here, however, the different details of the boundary layer formulation in Model E are apparent, as this model has higher velocities over land, but lower over many ocean grid boxes, again independent of vertical resolution issues.

3.4. Transport From the Troposphere Into the Stratosphere

[45] A number of the tracers have sources in the troposphere and primary sinks in the stratosphere. The ratio between their tropospheric and stratospheric burden is a

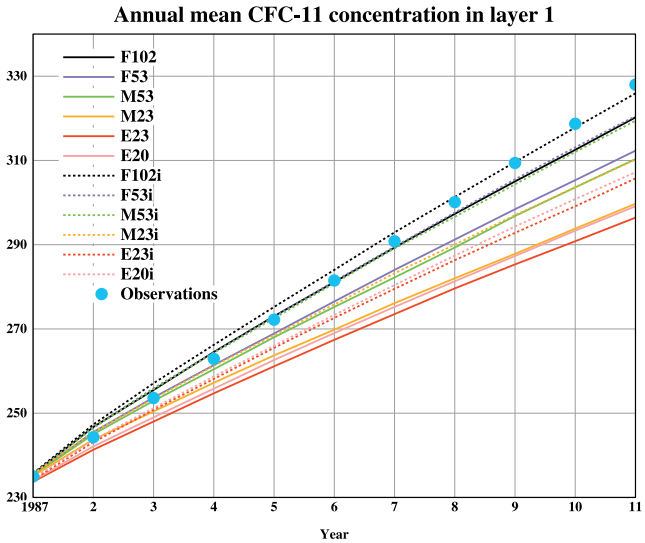

Figure 6. Trend in CFC-11 in the different GCM experiments compared with the average observed trend during the time of rapid source increase in the 1980s [*Kaye et al.*, 1994]. Observed trend is 9.3 pptv yr^{-1}.

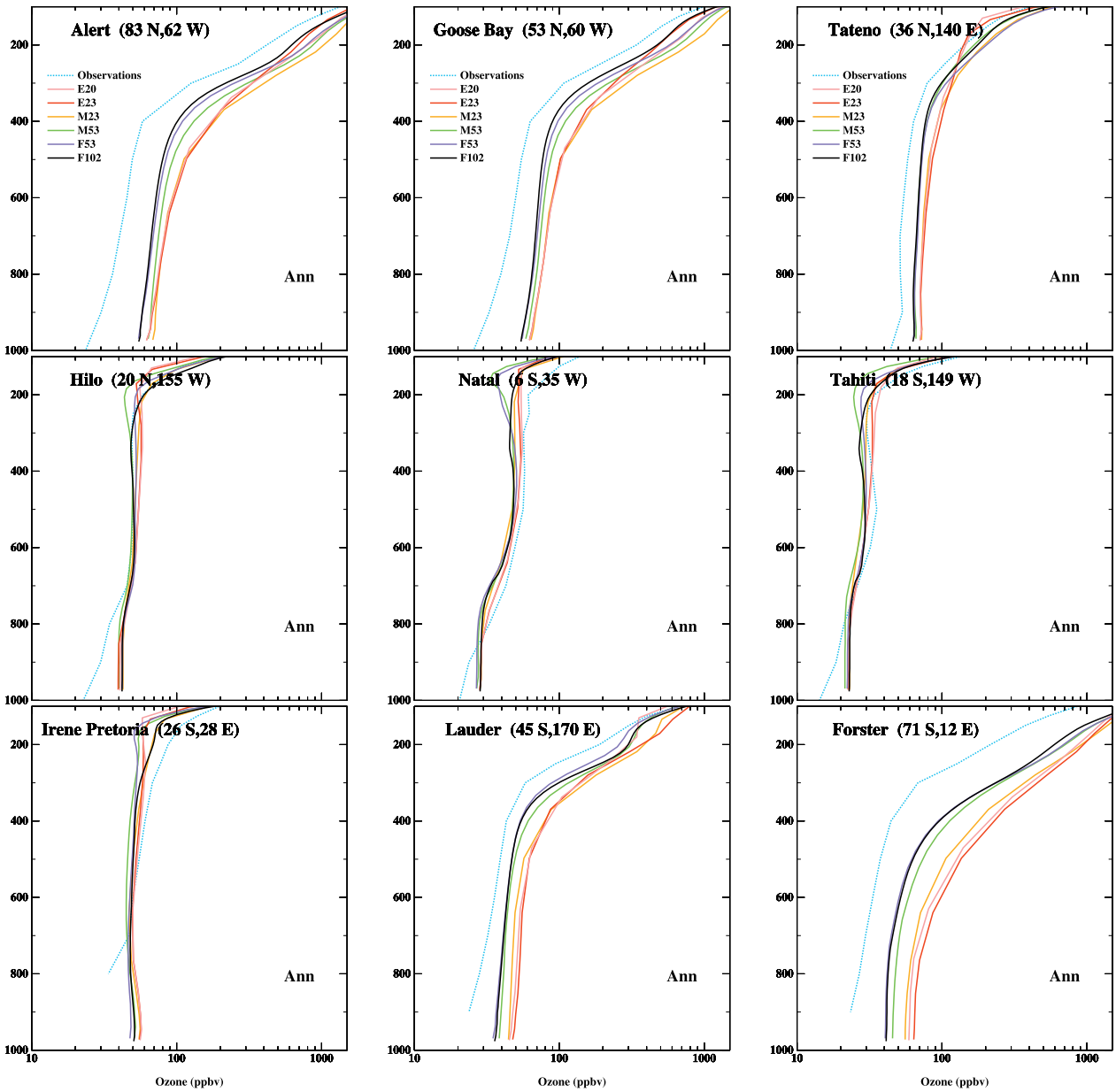

Figure 7. Annual average modeled tropospheric ozone profiles compared with ozonesonde data for stations at various latitudes. Results are indicative of those for other stations at the respective latitudes.

measure of the transport from the lower to the upper region. Shown in Table 5 are the ratios for three different species, CFC-11, CH_4 and N_2O. These all have somewhat different geographic source regions, and sinks at different altitudes within the stratosphere (in addition to the tropospheric sink/source for CH_4). Also shown are the results for SF_6 with a source in the lower troposphere and no stratospheric sink.

[46] The model E runs tend to have somewhat higher stratospheric concentrations, indicating faster transport from the troposphere to stratosphere. This would be expected of Model E because of its coarse resolution with its implicit vertical diffusion (see Table 1; the modeling layering varies smoothly so there is no special resolution near the tropopause different from that in the regions as a whole). However, the QUS scheme to some extent minimizes diffusive transports, and at the same resolution, E23 has consistently higher stratospheric concentrations than M23. The latitudinal distribution of the vertical transport of SF_6 through the 117 mbar level is presented in Figure 4; for comparison, we also show the vertical transport of a different species, CO_2. The differences among the models are clearly not a function of one specific species, as they are essentially the same for each of the species in Figure 4 and Table 5. The biggest differences in the transport into the stratosphere occur in the tropical region where there is a tendency for the finer resolution models to have less positive, or even negative transport right near the equator. In contrast, E23 has very large positive transports there.

[47] From the TEM perspective, the flux up through the tropical tropopause is associated with the large-scale residual

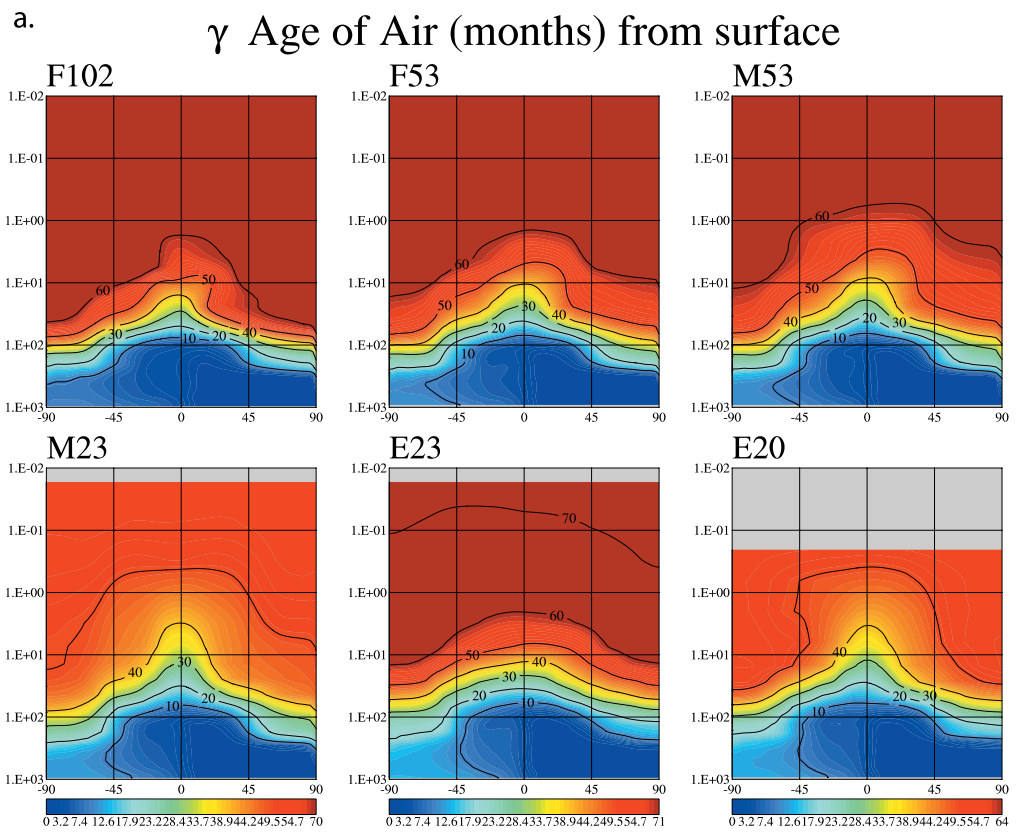

Figure 8. (a) Age of air derived from the SF_6 tracer by comparison with the concentration increase at the surface in the noninteractive (prescribed ozone) runs. (b) Change of age of air between the interactive ozone runs and the prescribed runs.

Table 7. Ratio of SF_6 Concentration at 2°N/30°N or 2°S/30°S at Different Pressure Levels in the Low to Middle Stratosphere[a]

	F102		F53		M53		M23		E23		E20	
Pressure, mbar	NH	SH	NH	SH	NH	SH	NH	SH	NH	SH	NH	SH
100	1.06 [1.07]	1.07 [1.09]	1.05 [1.05]	1.07 [1.09]	1.05 [1.06]	1.06 [1.08]	1.04 [1.05]	1.05 [1.07]	1.02 [1.02]	1.05 [1.06]	1.00 [1.01]	1.03 [1.04]
70	1.17 [1.19]	1.12 [1.20]	1.13 [1.18]	1.12 [1.21]	1.11 [1.16]	1.10 [1.19]	1.08 [1.13]	1.08 [1.15]	1.08 [1.08]	1.06 [1.11]	1.03 [1.06]	1.04 [1.06]
45	1.38 [1.39]	1.23 [1.39]	1.25 [1.33]	1.19 [1.35]	1.26 [1.33]	1.20 [1.36]	1.21 [1.27]	1.17 [1.31]	1.15 [1.16]	1.08 [1.15]	1.15 [1.21]	1.10 [1.19]
25	1.49 [1.51]	1.31 [1.48]	1.35 [1.37]	1.25 [1.35]	1.38 [1.41]	1.27 [1.41]	1.32 [1.35]	1.23 [1.33]	1.16 [1.14]	1.08 [1.11]	1.28 [1.36]	1.20 [1.26]

[a]The larger the ratio, the less "leaky" is the stratospheric tropical "pipe." Results from the "interactive" runs are shown in brackets.

(Brewer-Dobson) circulation in the upper troposphere/lower stratosphere, itself driven by wave flux (Eliassen-Palm) convergences ($-\nabla \bullet EP$). There is a correspondence between the $-\nabla \bullet EP$ and the ordering in Table 5, as Model E has the largest values in the lower stratosphere, and the finer grid runs have the smallest. Differences amongst the models in both physics and resolution are involved; we provide a fuller discussion in Section 3.5.

[48] Additional insight can be found by investigating the longitudinal variations associated with the zonal average. The differences relate to the vertical velocity and ultimately to the tropical eddy kinetic energy. Eddy heat flux divergence around the equator is providing cooling, and inducing subsidence at 100 mbar in the finer resolution models, especially over the western Pacific. With the greater tropical eddy kinetic energy in F102 (Table 2), there is greater cooling due to eddy heat flux divergence at the 100 mbar level (-0.6°C d^{-1}) compared to E23 (0.0°C d^{-1}) and E20 (-0.1°C d^{-1}) both of which had the least eddy kinetic energy (Table 2); M53, with the next most eddy kinetic energy, had the next higher eddy heat flux divergence (-0.4°C d^{-1}) (in F53 it was -0.3°C d^{-1}). (Note: the eddy-induced temperature differences are not compensated for by mean circulation effects, which are promoting a similar smaller cooling in each run.) These longitudinally specific effects are in addition to the zonal mean residual circulation forcing ($\nabla \bullet EP$) discussed above. This effect of increased eddy heat transport divergences on decreasing the vertical transport into the stratosphere by producing cooling and subsidence is contrary to the mechanism proposed by *Reid and Gage* [1996], in which eddy heat transports would amplify the vertical transport by altering the stability profile to allow for more convective overshooting.

[49] Another factor influencing the net vertical transport, and hence the results in Table 5, is the transport downward back into the troposphere in the vicinity of the subtropical jet. As implied by the transports in Figure 4, all the models exhibit the well-known thermally direct circulation with rising motion equatorward of the subtropical jet, and sinking motion poleward, but the result in E23 is quite anomalous, with very strong downward and upward transports in the vicinity of the jet. It is associated with an oscillation in the mean circulation (it does not show up in the eddy transports), and extends throughout the troposphere. It appears to be the result of the (orographic) gravity wave drag parameterization, which has a similar variation associated with topography, i.e., its impact oscillating with latitude, and resulting in alternating convergences and divergences. E23 has the strongest gravity wave drag in the lower stratosphere, which appears to contribute to this circulation (E20 with Rayleigh friction acting everywhere does not have the latitudinal dependence). Even averaging out the oscillations, E23 has considerably larger downward SF_6 transport in the vicinity of the subtropical jets, to balance its increased vertical transport through the equatorial region.

[50] To verify that the strong parameterized orographic drag was responsible for the results shown in Figure 4, we reran E23 for 12 years with the reduced parameterized orographic momentum flux that is employed in M23; the strong oscillation in transports disappeared. In addition, the

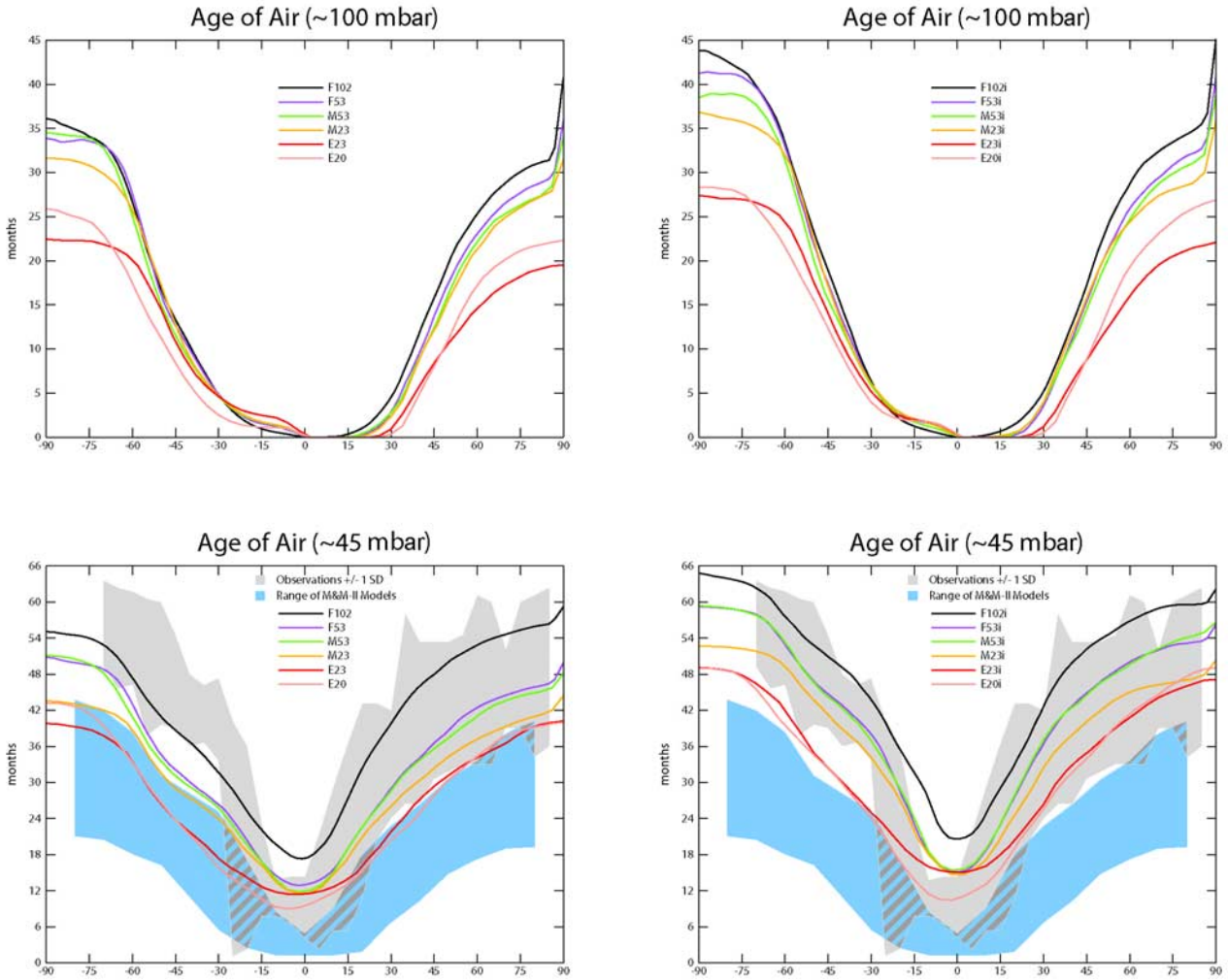

Figure 9. Age of air at (top) 100 mbar and (bottom) 45 mbar for the (left) noninteractive runs and (right) interactive runs calculated by comparison with the concentration at the tropical tropopause. In the bottom plots, model results are compared with observations [*Andrews et al.*, 2001] and the range of M&M II models [*Hall et al.*, 1999].

upward transport through the tropics was reduced, closer to the values in M23.

[51] What is the proper ratio of concentrations above/below 100 mbar? We can estimate that value using nine years of the HALEO-CLAES stratospheric methane observations along with general observations of tropospheric methane. The ratio for CH_4 corresponding to the values in Table 5 is 8.9. From that perspective, the ratio in F102 looks to be too low, while that of E23 is too high. However, we can also compare the variation with time of a species whose primary loss mechanism is via transport into the stratosphere. We use CFC-11 during the time when the trend was strong which corresponds to the increase in source strength used in these experiments. The observed increase was 9.3 pptv yr^{-1} during the 1980s [*Cunnold et al.*, 1994; *Kaye et al.*, 1994]; the model results compared with this trend are shown in Figure 5. The models with the smallest flux into the troposphere best fit the observed trend, and in this case F102i looks to be the best.

3.5. Transport From the Stratosphere Into the Troposphere

[52] In conjunction with the previous section, a more rapid rate of upward transport should be associated with more rapid downward transport. The location of the downward transport is also an issue, as transports into the troposphere at high latitudes are more protected in winter from active photochemistry.

[53] To assess downward transports, we use bomb ^{14}C, associated with the explosion of October 1963, the subject of a multimodel intercomparison [*Prather and Remsberg*, 1993]. We calculate the residence time via a linear fit to the logarithmic falloff of the stratospheric composition. The results are shown in Table 6 for both the first 36 months, and 7.5 years.

[54] The observed residence time varied with duration from the bomb release; as the time from the explosion increased, the atmospheric circulation was able to transport material to higher levels in the stratosphere, lengthening its

residence time. The short-term residence time was probably close to 4 years, while the longer time was on the order of 5 years [*Prather and Remsberg*, 1993]. From that perspective, for the short term the finer resolution runs (especially F102) produced the most realistic result, while the coarser resolution models were the least realistic. On the longer timescale, F102 again was the most realistic, while the other models showed no systematic change with resolution.

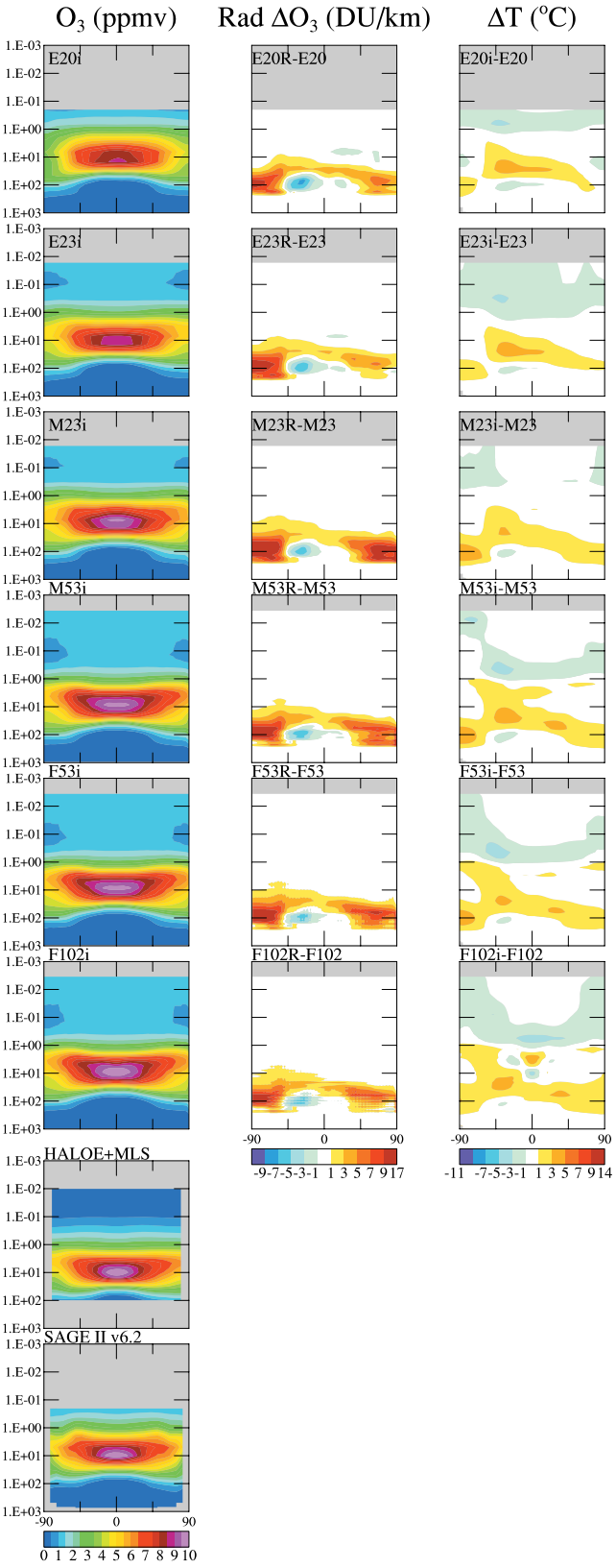

[55] Considering the mechanisms for downward transport, first from the TEM perspective, Model E has an intensified downward flow as part of its stronger residual circulation. We show in Figure 6 the residual circulation vertical velocity ($\overline{w}^*$) for the different models at the 100 mbar level. The model E values show greater downward flow in the extratropics of both hemispheres (as well as greater upward flow in the tropics). These larger values are driven by larger EP flux convergences in the lower stratosphere in model E, at least in part due to the stronger gravity wave drag in that model. In addition, E23 shows greater oscillations in $\overline{w}^*$ (as it did in the total transport of Figure 4), also associated with the stronger gravity wave drag. All the models have strong negative values of $\overline{w}^*$ near the poles worse in model E in the Southern Hemisphere (its $\overline{w}^*$ values go up to 2000×10^{-6} m s^{-1}), where its orographic gravity wave drag is stronger.

[56] From the standard Eulerian perspective, for Model 3, the finer resolution models have less eddy kinetic energy at the 100 mbar level, due to a reduction in upward flux of eddy geopotential energy (i.e., upward wave flux). Presumably with finer horizontal resolution, waves move further and transport heat poleward more efficiently, and as a concomitant, have reduced total upward energy flux. In addition, with finer vertical resolution, the reduction with altitude of eddy geopotential flux is better resolved, leading to less eddy kinetic energy around 100 mbar. The reduction in eddy kinetic energy then leads to reduced downward transport at upper midlatitudes. This reasoning also applies to the reduced EP flux convergences found in the lower stratosphere in the finer resolution runs, discussed in section 3.4 responsible for the weaker residual circulation.

[57] We can also evaluate the transport of ozone from the stratosphere into the troposphere. Also shown in Table 6 are the annual average values for the different models. The finer grid models have the smallest net transport. Observed ozone fluxes into the troposphere are generally in the range of 400–600 Tg yr^{-1} [*Murphy and Fahey*, 1994; *Olsen et al.*, 2001, 2004], while *Stevenson et al.* [2006] reported the average from 25 models of 520 ± 200. The finer resolution models are more consistent with this range, although an "observed" value as large as 800 Tg yr^{-1} results from using the extreme estimates for each hemisphere of *McLinden et al.* [2000].

[58] A further test of the validity of the ozone influx can be obtained by comparing the resulting tropospheric ozone profiles with observations. Shown in Figure 7 are comparisons with annual average observations for a range of

Figure 10. (left) Annual average ozone distribution in the different models for the interactive run as well as observations from SAGE II [*Rind et al.*, 2005] and HALOE-MLS (obtained from the SPARC data center). (middle) Difference in ozone between that calculated (and used for the radiation) in the interactive run and that specified from observations (and used for the radiation in the noninteractive run). (right) Annual average temperature difference between the interactive and noninteractive run.

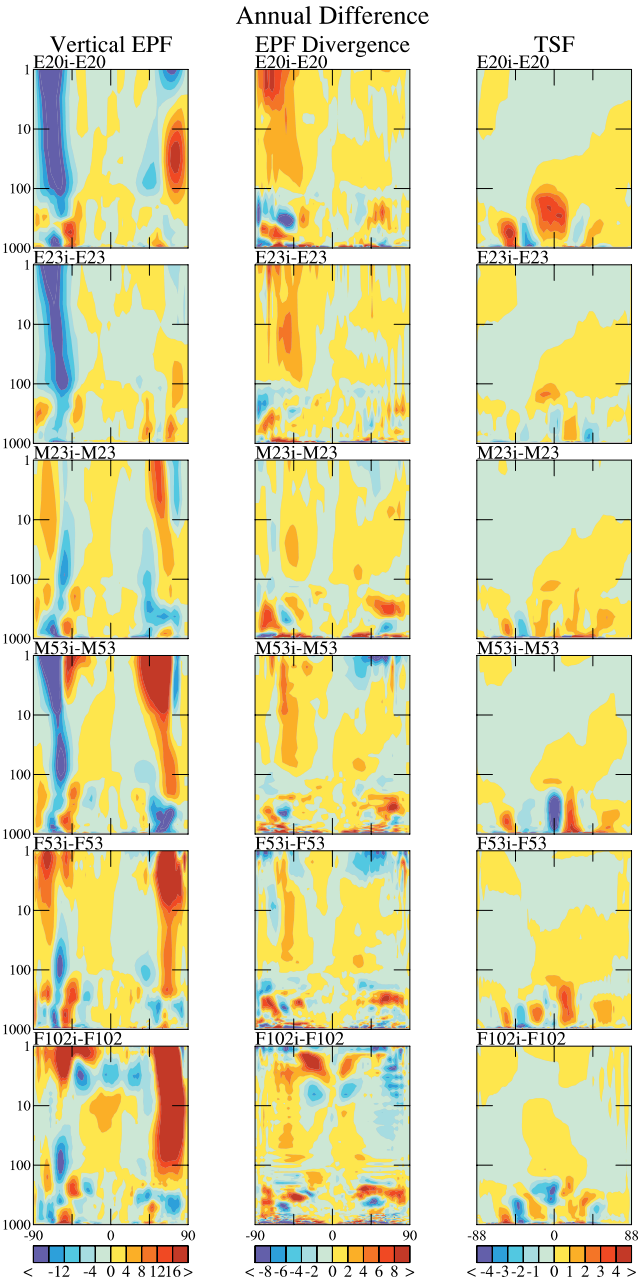

Figure 11. Annual difference between the interactive and noninteractive runs for (left) the vertical EP flux (10^{-3} m^2 s^{-2}), (middle) the EP flux divergence (10^{-6}m s^{-2}), and (right) the transformed (residual) stream function (10^9 kg s^{-1}).

latitudes (the same general characteristics exist in all seasons). These results are representative of other stations at the respective latitudes. As can be seen, the different models all produce excessive ozone at the higher latitudes, with the finer resolution runs producing the more realistic results in direct relationship to the relative influx of ozone (Table 5). The errors are less at midlatitudes and all the models produce reasonable distributions in the tropics.

[59] It is also apparent in Tables 5 and 6 that the interactive runs have smaller fluxes through the tropopause (and they have more realistic profiles compared with ozonesonde data, not shown). We discuss the reason for this in section 3.7.

3.6. Transport Within the Stratosphere

[60] A summary presentation of the rapidity of the stratospheric circulation is obtained by diagnosing the age of air. Presented in Figure 8a are the age of air profiles generated from calculating correlations with the SF_6 increase at the surface. The differences among the model circulations are apparent. E20 has the youngest air in the upper stratosphere, influenced by the presence of the model top. In general, the finest resolution models have the oldest age of air throughout the middle atmosphere, with the exception of E23, which, however, has the flattest distribution.

[61] The latitudinal spread in age of air contours is indicative of the most "leaky" stratospheric pipe. We quantify this aspect by relating the ratio of SF_6 in the tropics to the value at 30°N/S for various pressure levels in the low to middle stratosphere (Table 7). As is evident in Table 7, the finer resolution models in the low to middle stratosphere have less leaky tropical pipes, while the Model E values are more leaky. This can be related at least partly to the gravity wave drag parameterization in Model E (or Rayleigh friction in E20), which in the lower stratosphere (including the subtropics) is 10 times stronger than that in Model 3; when acting on a west wind, the drag forces a poleward flow which helps mix air out of the tropical pipe region. The rerun of E23 with reduced orographic gravity wave drag reduced the differences seen in Table 7 between E23 and M23 by about 1/2.

[62] We compare (Figure 9, left) the age of air in the models from SF_6 (calculated now with respect to the concentration in the tropical upper troposphere) with observations [*Andrews et al.*, 2001] and with models that participated in the M&M II simulations [*Hall et al.*, 1999] (Figure 9, bottom). The finer resolution models have larger values and, especially in the interactive runs (right), are within the range of the observations (which utilize CO_2, and produce results similar but probably not identical to those from SF_6). The model E values in general are too young. Compared with the models from the M&M II simulations, all Model 3 configurations produce older and more accurate age of air assessments in the extratropics.

[63] These differences relate directly to the different intensities and configurations of the residual circulation in the stratosphere, driven by the EP flux convergences discussed previously. If the absolute value of the annual average residual circulation intensity at 24N and 24S, 117 mbar are added together, the largest value is in E23 (20×10^9 kg s^{-1}), the next large in E20 (17×10^9 kg s^{-1}), the smallest in F102 (13×10^9 kg s^{-1}), and the next smallest in F53 (14×10^9 kg s^{-1}). The values for the interactive runs are generally about 1×10^9 kg s^{-1} lower. (Comparison with the results in Table 3 shows that the models with the weakest/strongest tropospheric Hadley cell have the strongest/weakest stratospheric residual circulation.)

3.7. Influence of Interactive Ozone

[64] Shown in Figure 8b is the difference in age of air between the runs which used the tracer-derived ozone in the atmospheric radiation calculations and the standard runs

which used observed ozone. In the stratosphere, the interactive runs show increased ages of air, sometimes exceeding one year. Comparison with observations (Figure 9, right) shows that these ages of air are more accurate. In the previous sections, it was apparent in the tables that the interactive ozone runs had reduced transports in and out of the stratosphere, and looked more realistic. Why were the interactive runs more successful in simulating transports associated with upper tropospheric and stratospheric processes?

[65] The ozone distribution produced in the interactive runs is shown in Figure 10 (left plots, along with observations from SAGE II and HALOE-MLS). In the middle plots of Figure 10 we show the difference with the specified ozone used in the noninteractive runs, derived from numerous sources including a zonally averaged monthly mean climatology constructed by G. Labow (personal communication, 2004) from ozonesonde observations, merged with SAGE II and UARS-MLS data [*Schmidt et al.*, 2006]. The ''prescribed'' versus ''tracer'' ozone difference indicates the interactive runs have more ozone in the lower stratosphere, especially at higher latitudes. A primary reason for most if not all of this discrepancy, which is generally on the order of 30–40% annually, is that the Linoz scheme as utilized does not contain an ozone hole parameterization; the model results therefore look much more like the pre-1980s ozone values in these regions. With the added ozone, the interactive run features warmer temperatures in the polar regions (Figure 10, right plots). The warming of some 5°C averaged over Southern Hemisphere summer is consistent with that calculated for this season poleward of 65°S due to the ozone hole in the Hadley Centre model and is in general agreement with observations [*Gillett and Thompson*, 2003]. The warming is less in the Northern Hemisphere during summer due to the weaker ozone hole.

[66] The warmer temperatures lead to increased stability and reduced eddy kinetic energy generation. Shown in Figure 11 is the annual average difference in the vertical EP flux between the interactive and noninteractive runs (left), the difference in EP flux divergence (EPFD) (middle) and the difference in the transformed Eulerian (residual) stream function (TSF) (right). For stratospheric age of air considerations, the region of prime concern is between 100 and 10 mbar. In both hemispheres, at most latitudes but particularly in the extratropics, all the interactive runs feature a reduction of planetary wave energy, with peak values in the stratosphere of 20–30%. The result of this reduction is a relative increase in EFPD between 100 and 10 mbar, again of order 20–30%. With an increase in EFPD, the stratospheric residual circulation is driven less strongly, and slows down (positive values in the Northern Hemisphere and negative values in the Southern Hemisphere for the TSF change are opposite to the control run values, and hence indicate a weakening of the circulation). The TSF reduction signifies a reduction in $\overline{w}^*$ and $\overline{v}^*$, the effective vertical and meridional transport velocities for tracers, resulting in the increased age of air. The difference in the EFPD increase in the two hemispheres (Figure 11, middle) also results in a more symmetrical distribution of tracer ages around the equator.

[67] The upward EP wave flux from the troposphere, especially in the Southern Hemisphere, is reduced on the order of 10–15%. This occurs in all the models in approximately the same way. The effect starts at the surface (especially in the Southern Hemisphere), weakens in the middle troposphere, and then arises again directly from the upper troposphere where the effect of the stability increase is most felt. Hence the interactive stratospheric ozone run has altered the wave energy forcing from the troposphere, affecting the age of air in the stratosphere. The peak eddy kinetic energy changes in the troposphere itself are a few percent.

[68] The warmer polar temperatures (which occur primarily in summer, especially in the Southern Hemisphere) actually correct a long-standing model problem, true for most GCMs [e.g., *Roeckner et al.*, 2006]: the inability to produce sufficiently high temperatures at high Southern latitudes in the upper troposphere/lower stratosphere during summer. By alleviating this problem, the interactive run produced a more realistic circulation.

4. Discussion and Conclusions

[69] The prime purpose of this comparison has been to determine if model physics, vertical resolution or horizontal resolution affect the different tracer transport characteristics in models, discussed here with respect to the new GISS GCMs. The primary conclusions are as follows:

[70] 1. Model physics: The cloud and convection schemes affect precipitation over land, and this has a noticeable impact on interhemispheric transport. Lack of sufficient precipitation over land in the monsoon region during Northern Hemisphere summer in Model E results in IHT that appears to be too slow. By affecting tropical eddy kinetic energy, it also results in faster transport through the tropical tropopause. Smaller changes arise in the vertical transport within the troposphere. Differences in the boundary layer scheme (*not* using virtual potential temperature) at least in part allow Model E to produce diurnal variations and boundary layer processes as good as the finer resolution models. The strong gravity wave drag in the lower stratosphere results in excessive leakiness of the stratospheric tropical pipe, and large (spurious) transport in, within and out of the stratosphere. Having the model top near the stratopause reduces the age of air to unrealistic values there.

[71] 2. Horizontal resolution: Most of the transport characteristics do not appear to be dependent on horizontal resolution in this range, at least when the same vertical resolution is used (M53, F53); for example, there are similar interhemispheric transports, similar percentage of eddy/MMC contribution to the IHT, similar EKE and intrahemispheric transport, and generally similar vertical transport within the troposphere. Within the stratosphere, the leakiness of the tropical pipe is similar, as is the age of air. F53 has slightly smaller transport between the troposphere and stratosphere and slightly longer residence time for bomb ^{14}C within the stratosphere.

[72] However, it is important to note that horizontal resolution has been found to have significant impact on photochemistry. For example, *Wild and Prather* [2006] showed how tropospheric ozone production is dependent on model resolution because its chemistry is nonlinear, the timescales for chemical production are short, and precursors are artificially distributed over the spatial scale of the model

grid. In particular, ozone production is larger at coarser resolution where urban and rural emissions are artificially mixed. Chemical model comparisons may thus differ because of different horizontal resolutions for reasons other than their transport properties.

[73] 3. Vertical resolution: In contrast, vertical resolution has noticeable impact on tracer transports. The finer vertical resolution runs have faster interhemispheric transport (associated with both stronger Hadley circulation and increased tropical eddy kinetic energy), somewhat increased vertical mixing in the troposphere, slower transport between the troposphere and stratosphere, older age of air, and a less leaky stratospheric tropical pipe. Boundary layer processes are actually much less affected, contrary to expectation.

[74] The combined increase in vertical and horizontal resolution in F102 does have effects that are not apparent when just horizontal resolution is increased; in particular the tropical EKE is much larger, the moist convective transports do not reach to as high an level, and there are some differences in the boundary layer concentrations of ^{222}Rn. *Lindzen and Fox-Rabinovitz* [1989] discussed ways to assess the horizontal and vertical scaling necessary to represent atmospheric waves accurately and avoid noise in simulations, by comparison to the Rossby ratio between horizontal and vertical scales in quasigeostrophic flow and the dispersion relation for internal gravity waves. While the values vary with latitude and type of wave, from the work of *Pope et al.* [2001] it can be noted that for 45° latitude, vertical resolution of 2 km is appropriate for resolutions on the order of 4° × 5°; this value is exceeded slightly in E20 and is greater than that found in the 23 layer or 53 layer models. For a resolution of 2° × 2.5°, 1 km resolution is sufficient, and that is considerably larger than in F53 or F102. Thus these models would appear to have vertical resolution at least sufficient for the horizontal resolution employed. However, the scaling breaks down in the tropics, and previous studies have shown the tropical response, including both convection and the Hadley Circulation, is highly sensitive to vertical resolution [*Williamson*, 1999; *Pope et al.*, 2001; *Roeckner et al.*, 2006]. The results here show that the significant differences which exist between F102 and the other models are often associated with its tropical response.

[75] 4. Effect of interactive ozone: By changing the temperature structure in the lower, stratosphere, transports into, within and out of the stratosphere were all affected to a surprisingly large degree. This process acts through altering the wave generation in the troposphere and its flux into the stratosphere. This large sensitivity illustrates the strong feedback that stratospheric ozone changes can have on stratospheric and related transports, operating via a tropospheric forcing mechanism; it has implications for the ability of climate perturbations to affect the stratosphere. It also suggests that the stratosphere prior to 1980 would have had a reduced residual circulation and increased age of air. As the ozone hole gradually diminishes in the future, this component will tend to increase the age of air, an effect that would have to be compared with the influence of increasing CO_2.

[76] For the sake of GCM transports, these studies suggest the following prescriptions for model development: (1) Tropical precipitation over land is of utmost important and changes in convective, boundary layer and cloud cover parameterizations should be gauged by how they alter this field; (2) models should use as small magnitudes of gravity wave drag in the lower stratosphere as possible; (3) increases in vertical resolution are more important than horizontal resolution for tracer transport (not considering photochemistry); and (4) it is important to improve the simulation of summer temperatures in the upper troposphere/lower stratosphere, especially in the Southern Hemisphere for the sake of more realistic tracer circulation in the stratosphere. While these conclusions have been derived on the basis of various GISS GCM configurations, at least some of these results should prove relevant to general model intercomparisons of tracer transports.

[77] **Acknowledgments.** We thank Loretta Mickley for help with the tropospheric ozone parameterization and observations, as well as useful comments in review. This work was supported by grants from the NASA Atmospheric Composition focus area, the NASA CACTUS IDS grant, an EPA GCAP grant, and the NASA NCCS high-speed computing center. Climate modeling at GISS is supported by the NASA Climate Variability and Climate Change focus area.

References

Andrews, A. E., et al. (2001), Mean ages of stratospheric air derived from CO_2, CH_4 and N_2O, *J. Geophys. Res.*, *106*, 32,295–32,314.

Andrews, D. G., and M. E. McIntyre (1976), Planetary waves in horizontal and vertical shear: The generalized Eliassen-Palm relation and the mean zonal acceleration, *J. Atmos. Sci.*, *33*, 175–185.

Andrews, D. G., J. R. Holton, and C. B. Leovy (1987), *Middle Atmosphere Dynamics*, *Int. Geophys. Ser.*, vol. 40, 489 pp., Elsevier, New York.

Beck, C., J. Grieser, B. Rudolf, and U. Schneider (2005), A new monthly precipitation climatology for the global land areas for the period 1951 to 2000, *Geophys. Res. Abstr.*, *7*, 07154.

Bey, I., D. J. Jacob, R. M. Yantosca, J. A. Logan, B. D. Feld, A. M. Fiore, Q. Li, H. Liu, L. J. Mickley, and M. Schultz (2001), Global modeling of tropospheric chemistry with assimilated meteorology: Model description and evaluation, *J. Geophys. Res.*, *106*, 23,073–23,096.

Boer, G. J., and B. Denis (1997), Numerical convergence of the dynamics of a GCM, *Clim. Dyn.*, *13*, 359–374.

Boer, G. J., and M. Lazare (1988), Some results concerning the effect of horizontal resolution and gravity wave drag on simulated climate, *J. Clim.*, *1*, 789–806.

Boville, B. A. (1991), Sensitivity of simulated climate to model resolution, *J. Clim.*, *4*, 469–485.

Boyle, J. S. (1993), Sensitivity of dynamical quantities to horizontal resolution for a climate simulation using the ECMWF (cycle 33) model, *J. Clim.*, *6*, 796–815.

Brankovic, C., and D. Gregory (2001), Impact of horizontal resolution on seasonal integrations, *Clim. Dyn.*, *18*, 123–143.

Canuto, V. M., and M. S. Dubovikov (1996a), A dynamical model for turbulence, I. General formalism, *Phys. Fluids*, *8*, 571–586.

Canuto, V. M., and M. S. Dubovikov (1996b), A dynamical model for turbulence, II. Shear-driven flows, *Phys. Fluids*, *8*, 587–598.

Chen, T.-C., and J. J. Tribbia (1993), An effect of the model's horizontal resolution on stationary eddies simulated by the NCAR CCM1, *J. Clim.*, *6*, 1657–1664.

Cheng, Y., V. A. Canuto, and A. M. Howard (2002), An improved model for the turbulent PBL, *J. Atmos. Sci.*, *59*, 1550–1565.

Crawford, S. L., and T. Sasamori (1981), A study of the sensitivity of the winter mean meridional circulation to sources of heat and momentum, *Tellus*, *33*, 340–350.

Cunnold, D., P. Fraser, R. Prinn, P. Simmonds, F. Alyea, R. Weiss, A. Crawford, and F. Alyea (1994), Global trends and annual releases of CCl3F and CCl2F2 estimated from ALE/GAGE measurements from July 1978 to June 1991, *J. Geophys. Res.*, *99*, 1107–1126.

Denning, A. S., et al. (1999), Three-dimensional transport and concentration of SF6—A model intercomparison study (TransCom 2), *Tellus, Ser. B*, *51*, 266–297.

Dentener, F., et al. (2006), The global atmospheric environment for the next generation, *Environ. Sci. Technol.*, *40*, 3586–3594.

Deque, M., C. Dreveton, A. Braun, and D. Cariolle (1994), The ARPEGE/IFS atmosphere model: A contribution to the French community climate modeling, *Clim. Dyn.*, *10*, 249–266.

Fung, I., J. John, J. Lerner, E. Matthews, M. Prather, L. P. Steele, and P. J. Fraser (1991), Three-dimensional model synthesis of the global methane cycle, *J. Geophys. Res.*, *96*, 13,033–13,065.

Gillett, N. P., and D. W. J. Thompson (2003), Simulation of recent Southern Hemisphere climate change, *Science*, *302*, 273–275.

Gilliland, A. B. (1997), Potential influences of ENSO on interhemispheric transport, Ph.D. thesis, Ga. Inst. of Technol., Atlanta.

Gleckler, P. J., and K. E. Taylor (1993), The effect of horizontal resolution on ocean surface fluxes in the ECMWF model, *Clim. Dyn.*, *9*, 17–32.

Hall, T. M., D. W. Waugh, K. A. Boering, and R. A. Plumb (1999), Evaluation of transport in stratospheric models, *J. Geophys. Res.*, *104*, 18,815–18,839.

Hannegan, B., S. Olsen, M. Prather, X. Zhu, D. Rind, and J. Lerner (1998), The dry stratosphere: A limit on cometary water influx, *Geophys. Res. Lett.*, *25*, 649–1652.

Hartley, D. E., and R. X. Black (1995), Mechanistic analysis of interhemispheric transport, *Geophys. Res. Lett.*, *22*, 2945–2948.

Hess, P. G. (2005), A comparison of two paradigms: The relative global roles of moist convective versus non-convective transport, *J. Geophys. Res.*, *110*, D20302, doi:10.1029/2004JD005456.

Holtslag, A. A. M., and C.-H. Moeng (1991), Eddy diffusivity and countergradient transport in the convective atmospheric boundary layer, *J. Atmos. Sci.*, *48*, 1690–1698.

Hulme, M. (1992), A 1951–80 global land precipitation climatology for the evaluation of general circulation models, *Clim. Dyn.*, *7*, 57–72.

Intergovernmental Panel on Climate Change (IPCC) (1995), *Climate Change 1994: Radiative Forcing of Climate Change and an Evaluation of the IPCC IS92 Emission Scenarios*, edited by J. T. Houghton, et al., Cambridge Univ. Press, New York.

Jacob, D. J., and M. J. Prather (1990), Radio-222 as a test of convective transport in a general circulation model, *Tellus, Ser. B*, *42*, 118–134.

Jacob, D. J., M. J. Prather, S. C. Wofsy, and M. B. McElroy (1987), Atmospheric distribution of ^{85}Kr simulated with a general circulation model, *J. Geophys. Res.*, *92*, 6614–6626.

Johnston, H. (1989), Evaluation of excess carbon 14 and strontium 90 data for suitability to test two-dimensional stratospheric models, *J. Geophys. Res.*, *94*, 18,485–18,493.

Kållberg, P., P. Berrisford, B. Hoskins, A. Simmmons, S. Uppala, S. Lamy-Thépaut, and R. Hine (2005), ERA-40 atlas, *ERA-40 Proj. Rep. Ser. 19*, 191 pp., Eur. Cent. for Medium Range Weather Forecasts, Reading, U. K. (Available at http://www.ecmwf.int/publications/library/do/references/show?id = 86620)

Kaye, J. A., S. A. Penkett, and F. M. Ormond (Eds.) (1994), Report on concentrations, lifetimes and trends of CFCs, halons and related species, *NASA Ref. Publ. 1339*, 169 pp., NASA, Washington, D. C.

Kiehl, J. T., and D. L. Williamson (1991), Dependence of cloud amount on horizontal resolution in the National Center for Atmospheric Research Community Climate Model, *J. Geophys. Res.*, *96*, 10,955–10,980.

Kjellstrom, E., J. Feichter, and G. Hoffman (2000), Transport of SF_6 and (CO_2) -C-14 in the atmospheric general circulation model ECHAM4, *Tellus, Ser. B*, *52*, 1–18.

Law, R., et al. (1996), Variations in modeled atmospheric transport of carbon dioxide and the consequences for CO_2 inversions, *Global Biogeochem. Cycles*, *10*, 783–796.

Legates, D. R., and C. J. Willmott (1990), Mean seasonal and spatial variability in gauge-corrected, global precipitation, *Int. J. Climatol.*, *10*, 111–127.

Levin, I., and V. Hesshaimer (1996), Refining of atmospheric transport model entries by the globally observed passive tracer distribution of 85 Kr and sulfur hexafluoride (SF6), *J. Geophys. Res.*, *101*, 16,745–16,755.

Lindzen, R., and M. Fox-Rabinovitz (1989), Consistent vertical and horizontal resolution, *Mon. Weather Rev.*, *117*, 2575–2583.

Lintner, B. R. (2003), Mechanisms of passive tracer interhemispheric transport: An analysis of model-derived and observational interhemispheric transport climatology and interannual variations, Ph.D. dissertation, 279 pp., Univ. of Calif., Berkeley.

Mahowald, N. M., P. J. Rasch, B. E. Eaton, S. Whittlestone, and R. G. Prinn (1997), Transport of ^{222}radon to the remote troposphere using the Model of Atmospheric Transport and Chemistry and assimilated winds from ECMWF and the National Center for Environmental Prediction/NCAR, *J. Geophys. Res.*, *102*, 28,139–28,152.

McLinden, C. A., S. C. Olsen, B. Hannegan, O. Wild, M. J. Prather, and J. Sundet (2000), Stratospheric ozone in 3-D models: A simple chemistry and the cross-tropopause flux, *J. Geophys. Res.*, *105*, 14,653–14,666.

Moeng, C.-H., and P. P. Sullivan (1994), A comparison of shear-and buoyancy-driven planetary boundary layer flows, *J. Atmos. Sci.*, *51*, 999–1022.

Murphy, D. M., and D. W. Fahey (1994), An estimate of the flux of stratospheric reactive nitrogen and ozone into the troposphere, *J. Geophys. Res.*, *99*, 5325–5332.

Olsen, M. A., M. R. Schoeberl, and A. R. Douglass (2004), Stratosphere-troposphere exchange of mass and ozone, *J. Geophys. Res.*, *109*, D24114, doi:10.1029/2004JD005186.

Olsen, S. C., C. A. McLinden, and M. J. Prather (2001), Stratospheric N_2O-NO_y system: Testing uncertainties in a three-dimensional framework, *J. Geophys. Res.*, *106*, 28,771–28,784.

Park, R. J., D. J. Jacob, B. D. Field, R. M. Yantosca, and M. Chin (2004), Natural and transboundary pollution influences on sulfate-nitrate-ammonium aerosols in the United States: Implications for policy, *J. Geophys. Res.*, *109*, D15204, doi:10.1029/2003JD004473.

Phillips, T. J., L. C. Corsetti, and S. L. Grotch (1995), The impact of horizontal resolution on moist processes in the ECMWF model, *Clim. Dyn.*, *11*, 85–102.

Plumb, R. A., and J. D. Mahlman (1987), The zonally averaged transport characteristics of the GFDL general circulation/transport model, *J. Atmos. Sci.*, *44*, 298–327.

Plumb, R. A., and D. D. McConalogue (1988), On the meridional structure of long-lived. tropospheric constituents, *J. Geophys. Res.*, *93*, 15,897–15,913.

Pope, V. D., J. A. Pamment, D. R. Jackson, and A. Slingo (2001), The representation of water vapor and its dependence on vertical resolution in the Hadley Centre climate model, *J. Clim.*, *14*, 3065–3085.

Prather, M. J. (1986), Numerical advection by conservation of second order moments, *J. Geophys. Res.*, *91*, 6671–6680.

Prather, M. J., and E. E. Remsberg (Eds.) (1993), The atmospheric effects of stratospheric aircraft: Report of the 1992 models and measurements workshop, *NASA Ref. Publ. 1292*, vol. 13, 764 pp., NASA, Washington, D. C.

Prather, M., M. McElroy, S. Wofsy, G. Russell, and D. Rind (1987), Chemistry of the global troposphere: Fluorocarbons as tracers of air motion, *J. Geophys. Res.*, *92*, 6579–6613.

Reid, G., and K. Gage (1996), The tropical tropopause over the western Pacific: Wave driving, convection, and the annual cycle, *J. Geophys. Res.*, *101*, 21,233–21,241.

Rind, D. (1988), Dependence of warm and cold climate depiction on climate model resolution, *J. Clim.*, *1*, 965–997.

Rind, D., and J. Lerner (1996), The use of on-line tracers as a diagnostic tool in GCM model development, *J. Geophys. Res.*, *101*, 12,667–12,683.

Rind, D., R. Suozzo, N. K. Balachandran, A. Lacis, and G. L. Russell (1988), The GISS Global Climate/Middle Atmosphere Model part I: Model structure and climatology, *J. Atmos. Sci.*, *45*, 329–370.

Rind, D., J. Lerner, K. Shah, and R. Suozzo (1999), Use of on-line tracers as a diagnostic tool in general circulation model development: 2. Transport between the troposphere and stratosphere, *J. Geophys. Res.*, *104*, 9151–9167.

Rind, D., J. Lerner, and C. McLinden (2001), Changes of tracer distributions in the doubled CO_2 climate, *J. Geophys. Res.*, *106*, 28,061–28,079.

Rind, D., J. Lerner, J. Perlwitz, C. McLinden, and M. Prather (2002), Sensitivity of tracer transports and stratospheric ozone to sea surface temperature patterns in the doubled CO_2 climate, *J. Geophys. Res.*, *107*(D24), 4800, doi:10.1029/2002JD002483.

Rind, D., J. Lerner, and J. Zawodny (2005), A complementary analysis for SAGE II data profiles, *Geophys. Res. Lett.*, *32*, L07812, doi:10.1029/2005GL022550.

Roeckner, E., R. Brokopf, M. Esch, M. Giorgetta, S. Hagemann, and L. Kornblueh (2006), Sensitivity of simulated climate to horizontal and vertical resolution in the ECHAM5 atmosphere model, *J. Clim.*, *19*, 3771–3791.

Schmidt, G. A., et al. (2006), Present day atmospheric simulations using GISS ModelE: Comparison to in-situ, satellite and reanalysis data, *J. Clim.*, *19*, 153–192, doi:10.1175/JCLI3612.1.

Shea, D. J. (1986), Climatological atlas: 1950–1979, *NCAR TN-269+STR*, Natl. Cent. for Atmos. Res., Boulder, Colo.

Sperber, K. R., S. Hameed, G. L. Potter, and J. S. Boyle (1994), Simulation of the northern summer monsoon in the ECMWF model: Sensitivity to horizontal resolution, *Mon. Weather Rev.*, *122*, 2461–2481.

Staudt, A. C., D. J. Jacob, J. A. Logan, D. Bachiochi, T. N. Krishnamurti, and G. W. Sachse (2001), Continental sources, transoceanic transport, and inter-hemispheric exchange of carbon monoxide over the Pacific, *J. Geophys. Res.*, *106*, 32,571–32,590.

Stendel, M., and E. Roeckner (1998), Impacts of horizontal resolution on simulated climate statistics in ECHAM4, *Max Planck Inst. Meteorol. Rep. 253*, 57 pp., Max Planck Inst. für Meteorol., Hamburg, Germany.

Stevenson, D. S., et al. (2006), Multimodel ensemble simulations of present-day and near-future tropospheric ozone, *J. Geophys. Res.*, *111*, D08301, doi:10.1029/2005JD006338.

Taguchi, S., I. Takao, and J. Moriizumi (2002), Evaluation of the atmospheric transport model NIRE-CTM-96 by using measured radon-222 concentrations, *Tellus, Ser. B*, *54*, 250–268.

Trenberth, K. E., D. P. Stepaniak, and J. M. Caron (2000), The global monsoon as seen through the divergent atmospheric circulation, *J. Clim.*, *13*, 3969–3993.

Tselioudis, G., and C. Jakob (2002), Evaluation of midlatitude cloud properties in a weather and a climate model: Dependence on dynamic regime and spatial resolution, *J. Geophys. Res.*, *107*(D24), 4781, doi:10.1029/2002JD002259.

Wild, O., and M. J. Prather (2006), Global tropospheric ozone modeling: Quantifying errors due to grid resolution, *J. Geophys. Res.*, *111*, D11305, doi:10.1029/2005JD006605.

Williamson, D. L. (1999), Convergence of atmospheric simulations with increasing horizontal resolution and fixed forcing scales, *Tellus, Ser. A*, *51*, 663–673.

Williamson, D. L., and J. G. Olsen (1998), A comparison of semi-Lagrangian and Eulerian polar climate simulations, *Mon. Weather Rev.*, *126*, 991–1000.

Williamson, D. L., J. T. Kiehl, and J. J. Hack (1995), Climate sensitivity of the NCAR Community Climate Model (CCM2) to horizontal resolution, *Clim. Dyn.*, *11*, 377–397.

Wu, S., L. J. Mickley, D. J. Jacob, J. A. Logan, R. M. Yantosca, and D. Rind (2007), Why are there large differences between models in global budgets of tropospheric ozone?, *J. Geophys. Res.*, *112*, D05302, doi:10.1029/2006JD007801.

J. Jonas, J. Lerner, C. McLinden, and D. Rind, NASA Goddard Institute for Space Studies, New York, NY 10025, USA. (drind@giss.nasa.gov)